# MOUNTAIN-PLAINS CONSORTIUM

**MPC 24-561** | K. Venayagamoorthy, D. Sanchez and S. Chen

## CRASH MODELING OF HIGH-PROFILE MOVING VEHICLES UNDER STRONG CROSSWINDS BASED ON COMPUTATIONAL FLUID DYNAMICS

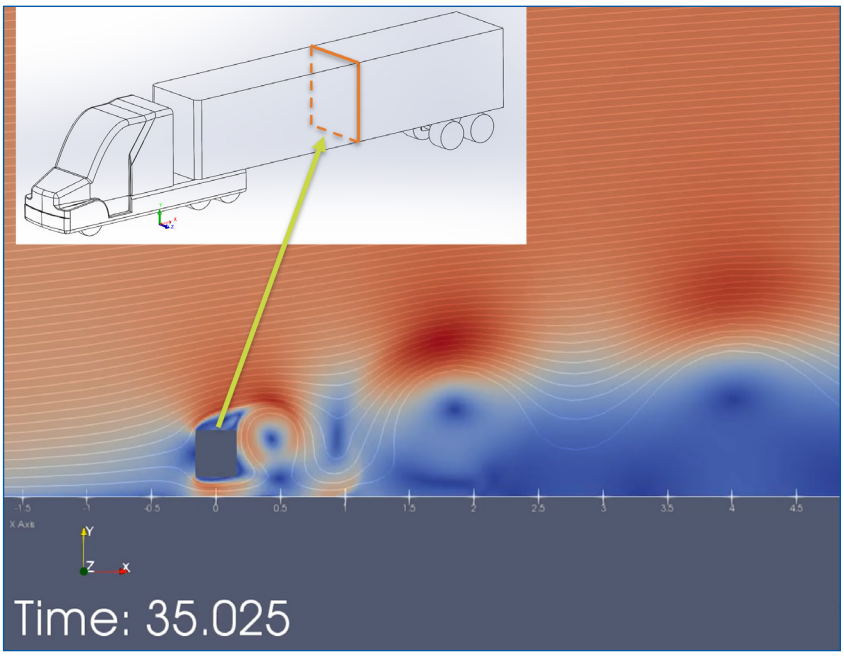


MOUNTAIN-PLAINS CONSORTIUM REGION 8

A University Transportation Center sponsored by the U.S. Department of Transportation serving the Mountain-Plains Region. Consortium members:

Colorado State University
North Dakota State University
South Dakota State University
University of Colorado Denver
University of Denver
University of Utah
Utah State University
University of Wyoming

**Technical Report Documentation Page**

| 1. Report No. | 2. Government Accession No. | 3. Recipient's Catalog No. |
|---|---|---|
| MPC-644 | | |

| 4. Title and Subtitle | 5. Report Date |
|---|---|
| Crash Modeling of High-Profile Moving Vehicles Under Strong Crosswinds Based on Computational Fluid Dynamics | September 2024 |
| | 6. Performing Organization Code |

| 7. Author(s) | 8. Performing Organization Report No. |
|---|---|
| Karan Venayagamoorthy<br>Daniel Sanchez<br>Suren Chen | MPC 24-561 |

| 9. Performing Organization Name and Address | 10. Work Unit No. (TRAIS) |
|---|---|
| Colorado State University<br>Department of Civil and Environmental Engineering<br>Fort Collins, CO 80523 | 11. Contract or Grant No. |

| 12. Sponsoring Agency Name and Address | 13. Type of Report and Period Covered |
|---|---|
| Mountain-Plains Consortium<br>North Dakota State University<br>PO Box 6050, Fargo, ND 58108 | Final Report |
| | 14. Sponsoring Agency Code |

15. Supplementary Notes

Supported by a grant from the US DOT, University Transportation Centers Program

16. Abstract

Extreme wind conditions can be a formidable foe to both highway and driver safety. Strong gusts increase the likelihood of wind-induced vehicle crashes, especially for high-sided vehicles (i.e., semi-trucks) in the United States. Current understanding of wind loads on high-sided vehicles comes mostly from wind tunnel tests, along with recent contributions from computational fluid dynamics (CFD) studies. However, limitations due to scaling issues (e.g., low Reynolds numbers) of wind tunnel data have constrained our understanding of the nature/uncertainties of such extreme load distributions due to high lateral wind conditions. In this research, we first conduct a comprehensive verification and validation (V&V) study of a CFD model. High-resolution CFD simulations are then used to investigate the flow around a two-dimensional rectangular cylinder that is representative of the trailer section of a high-sided vehicle. The findings of the study show that the flow past the trailer section of a high-sided vehicle is strongly asymmetrical and exhibits Reynolds number dependency compared with free flow around a rectangular cylinder. This contrasts with the assumption of a Reynolds number independence of aerodynamic coefficients made in traditional studies of overturning high-sided vehicles. The study also highlights the importance of ensuring that the model results are independent, not only of the grid sizing but also on the total domain sizing to obtain high fidelity results.

| 17. Key Word | 18. Distribution Statement |
|---|---|
| crosswinds, embankments, fluid dynamics, highway bridges, live loads, mathematical models, single vehicle crashes, traffic crashes, trucks, vehicle safety | Public distribution |

| 19. Security Classif. (of this report) | 20. Security Classif. (of this page) | 21. No. of Pages | 22. Price |
|---|---|---|---|
| Unclassified | Unclassified | 47 | n/a |

# Crash Modeling of High-Profile Moving Vehicles Under Strong Crosswinds Based on Computational Fluid Dynamics

Karan Venayagamoorthy (PI)

Daniel Sanchez (Graduate Research Assistant)

Suren Chen (Co-Investigator)

Department of Civil and Environmental Engineering
Colorado State University
Fort Collins, CO 80523

September 2024

## Acknowledgement

The authors thank the Mountain-Plains Consortium (MPC) for providing funds for this study through the United States Department of Transportation.

## Disclaimer

# ABSTRACT

Extreme wind conditions can be a formidable foe to both highway and driver safety. Strong gusts increase the likelihood of wind-induced vehicle crashes, especially for high-sided vehicles (i.e., semi-trucks) in the United States. Current understanding of wind loads on high-sided vehicles comes mostly from wind tunnel tests, along with recent contributions from computational fluid dynamics (CFD) studies. However, limitations due to scaling issues (e.g., low Reynolds numbers) of wind tunnel data have constrained our understanding of the nature/uncertainties of such extreme load distributions due to high lateral wind conditions. In this research, we first conduct a comprehensive verification and validation (V&V) study of a CFD model. High-resolution CFD simulations are then used to investigate the flow around a two-dimensional rectangular cylinder that is representative of the trailer section of a high-sided vehicle. The findings of the study show that the flow past the trailer section of a high-sided vehicle is strongly asymmetrical and exhibits Reynolds number dependency compared with free flow around a rectangular cylinder. This contrasts with the assumption of a Reynolds number independence of aerodynamic coefficients made in traditional studies of overturning high-sided vehicles. The study also highlights the importance of ensuring that the model results are independent, not only of the grid sizing but also on the total domain sizing to obtain high fidelity results.

# TABLE OF CONTENTS

# LIST OF TABLES

# LIST OF FIGURES

# EXECUTIVE SUMMARY

This report presents an investigation of high wind flow around a two-dimensional rectangular cylinder that represents a high-sided vehicle's trailer section using computational fluid dynamics (CFD) simulations. This study was motivated by the high crash risks posed by windstorms to vehicles on highways around the country. The study aims to provide fundamental insights into the flow dynamics around a high-sided vehicle under strong crosswinds.

Chapter 2 of this report provides a brief background on overturning high-sided vehicles with a focus on the aerodynamic coefficients of interest, including the rolling moment coefficient ($C_{rolling}$). Other important considerations pertaining to flow around high-sided vehicles are presented. Chapter 3 presents a detailed discussion on verification and validation of the CFD model study that was conducted to ensure the results are accurate. Chapter 4 includes a detailed discussion on the Reynolds number dependence of flow around a rectangular cylinder near a plane wall boundary, and the application to overturning high-sided vehicles are presented. The report concludes by providing a summary of the findings and recommendations for future research in Chapter 5.

This report highlights that verification and validation (V&V) are fundamental requirements for performing a successful CFD study for practical applications. It is common practice in CFD studies to assume that a grid (mesh) independence study is sufficient. However, this study highlights that for high Reynolds number incompressible flow, especially for flow around a bluff body (such as a high-sided vehicle) near a plane wall boundary (e.g., a road surface), it is critical to conduct a comprehensive verification analysis to ensure an adequate domain size is chosen such that it does not affect the flow dynamics.

For flow around rectangular cylinders, both in free flow and near a plane wall boundary, the drag coefficient has been evaluated at Reynolds numbers spanning from $10^4$ to $10^7$, filling a significant gap in this field of research. It has also been shown that there is a strong Reynolds number dependence for flow around a rectangular cylinder near a plane wall boundary. The application to overturning high-sided vehicles shows that the rolling moment coefficient ($C_{rolling}$) is Reynolds number dependent, which points to the need to reconsider the common assumption that aerodynamic coefficients are not Reynolds number dependent for high-sided vehicles.

# 1. INTRODUCTION AND LITERATURE REVIEW

## 1.1 Background

Extreme wind events such as thunderstorms, winter storms, and hurricanes pose high crash risks for vehicles on highways in the United States and beyond. In particular, high-sided vehicles (generally called semi-trucks in the U.S. or lorries in the British Isles are susceptible to overturning (rollover) crashes under high crosswinds, as illustrated in the time lapse photos in Figure 1. A recent example that occurred on September 9, 2020, involved the toppling of more than 45 semi-trucks in just a single day due to high winds in Utah (CNN 2020). A quick internet search will show that wind-induced vehicle crashes occur frequently across the country (e.g., TCPR 2018, WPTV 2019, NBC News 2017). Notwithstanding the implications of such crashes for the safety of drivers and other highway users, they also lead to extended highway closures, causing significant traffic disruptions and economic losses. Thus, efforts toward improved safety assessments and development of guidelines for management of traffic movement under extreme meteorological conditions should be undertaken.

**Figure 1.1 Sequence of a high-sided vehicle overturning under high crosswind (Images from The Weather Network)**

The likelihood of overturning a high-sided vehicle is typically evaluated using a predetermined rolling moment coefficient ($C_{rolling}$) to translate the wind speed into a rolling moment. This resulting rolling moment is then compared with the restoring moment to ascertain the force that would be required to overturn the high-sided vehicle. As such, this approach requires that $C_{rolling}$ be accurate with respect to the high-sided vehicle being evaluated. A recent study that provides a conglomeration of several studies investigating $C_{rolling}$ over the last 25 years shows the high uncertainty associated with $C_{rolling}$ (Baker and Soper, 2022), as shown in Figure 1.2. This figure shows the normalized rolling moment coefficient $C_{rolling}$ as a function of the relative angle of attack of the wind vector (also known as the yaw angle). Figure 1.2 shows a significant spread in the data for yaw angles between 45$^o$ and 90$^o$ (a direct crosswind), thereby increasing the uncertainty in the predicted wind speeds that might cause a vehicle to overturn.

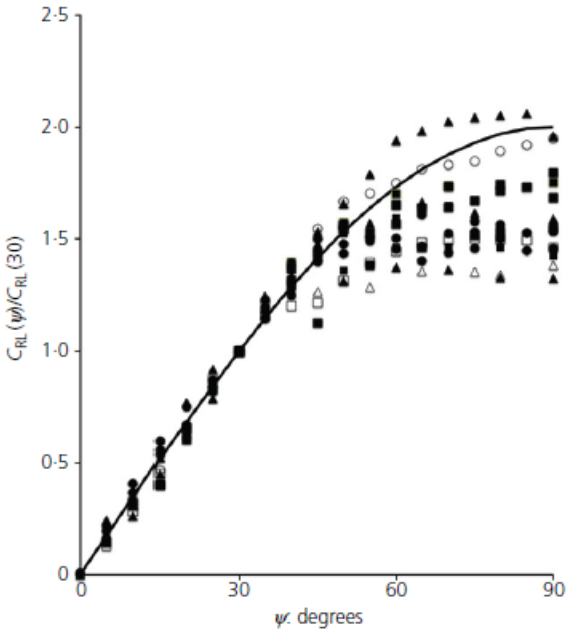


**Figure 1.2 The leeward normalized rolling moment coefficient $C_{rolling}$ plotted against the relative angle of attack of the wind, where 90° is a direct crosswind. Reproduced from Baker and Soper (2022)**

This uncertainty in $C_{rolling}$, especially under direct crosswind conditions, provides a strong impetus for this study, with a focus on understanding why the data spread is present and important. It is plausible that some of this variability may be attributed to the various high-sided vehicles used in the different studies; however, this may also be due to dependence on Reynolds number of the flow, a key finding of the present study. Here the Reynolds number (Re) of the flow is a nondimensional parameter that compares the inertial forces to the viscous forces in the flow. It can be simply expressed as $Re = VH/\nu$, where $V$ is the relative wind velocity encountering the object (vehicle), $H$ is the height of the vehicle (perpendicular to the wind) and $\nu$ is the kinematic viscosity of air.

## 1.2 Research Objectives

The overall goal of this research study is to provide new insights and understanding of the flow around a high-sided vehicle encountering strong crosswinds. There are two main objectives designed to meet this goal:

1. Develop a framework for comprehensive verification and validation (V&V) of a computational fluid dynamics (CFD) model for investigation of high Reynolds number flow around bluff bodies. Verification and validation are key components to performing a quality CFD study.

2. Conduct a high Reynolds number CFD study of incompressible flow around a rectangular cylinder near a plane wall with application to overturning high-sided vehicles. This study highlights how the assumption of Reynolds number independence of aerodynamic coefficients in traditional studies of overturning high-sided vehicles is questionable.

## 1.3 Organization of This Report

The layout of this report is as follows: Chapter 2 offers an overview of the CFD method, the setup of the CFD model, and the parametric framework employed in the study. Chapter 3 presents the verification and validation (V&V) study. Chapter 4 details the results and discussion concerning the Reynolds number dependency for flow around a rectangular cylinder near a planar wall boundary, as well as its application to overturning high-sided vehicles. Chapter 5 concludes with a summary of findings and recommendations for future research.

# 2. LITERATURE REVIEW

This chapter provides a brief review of the important facets pertaining to research of high-sided vehicles and flow around a rectangular cylinder near a plane wall boundary. A more comprehensive review is provided in the work by Sanchez (2023).

## 2.1 Background of Overturning of High-sided Vehicles

The field of research of wind effects on high-sided vehicles is young compared with other aspects of knowledge pertaining to flow around immersed (also known as bluff) bodies. The majority of existing research has been conducted in the European Union (EU). Trucking in the U.S. became more common following passage of the National Interstate and Defense Highway Act of 1956 (Hale 2015). Much of the research since that time has focused on fuel efficiency of high-sided vehicles, which has a primary emphasis on headwinds. The field of research into overturning of high-sided vehicles was pioneered by C.J. Baker of the United Kingdom (Baker 1986). It was clear that data on wind effects on ground vehicles were lacking (Baker 1991). Most of the earlier work by Baker and other researchers in the field focused on using wind tunnel models, but more recent studies have begun to include computational fluid dynamics (CFD) models. Some notable studies include those by Coleman and Baker (1990, 1994) and Cheli et al. (2011), where a framework was developed to investigate the overall system force and moment balance on a high-sided vehicle. These approaches typically make use of experimentally determined aerodynamic coefficients that vary on the yaw angle of vehicle and the specific vehicle type. The recent review article by Baker and Soper (2022) provides a good summary of different studies in various experimental settings, including wind tunnels, full-scale model tests, and CFD simulations. These aerodynamic coefficients include those related to lift, drag, sideslip, rolling moment, pitching moment, and yawing moment, which are discussed next.

## 2.2 Aerodynamic Coefficients

The main aerodynamic coefficients used in studies of high-sided vehicles are the drag coefficient ($C_{drag}$), side coefficient ($C_{side}$), lift coefficient ($C_{lift}$), and rolling moment coefficient ($C_{rolling}$) and are defined in equations (2.1) –(2.4) (see also Blevins 1984, Sterling et al., 2010, Baker and Humphreys 1996, Baker and Sopper 2022).

$$C_{drag} = \frac{F_D}{0.5\rho A V_r^2}, \tag{2.1}$$

$$C_{side} = \frac{F_S}{0.5\rho A V_r^2}, \tag{2.2}$$

$$C_{lift} = \frac{F_L}{0.5\rho A V_r^2}, \tag{2.3}$$

$$C_{rolling} = \frac{R_L}{0.5\rho A h V_r^2}, \tag{2.4}$$

where $F_D$ are drag forces exerted on the entire body, $F_S$ and $F_L$ are the forces exhibited on the reference area, $A$. $R_L$ is the overturning moment on a vehicle taken about the leeward wheels, $h$ is the reference height, and $V_r$ is the wind velocity relative to the vehicle.

## 2.3 U.S. Definition of and Focus on Overturning of High-sided Vehicles

Note the geometric variations of high-sided vehicles throughout the world and within local geographical locations. The physical differences of tractors and trailers is primarily due to the influence of the EU and U.S. and their respective regulations. The fundamental difference between U.S. and EU regulations pertains to how the maximum vehicle length is defined, as shown in Figure 2.1. In the U.S., the length of the trailer is restricted (USDOT 2004), whereas in the EU, the total length of the tractor-trailer is restricted (UK Government 2017).

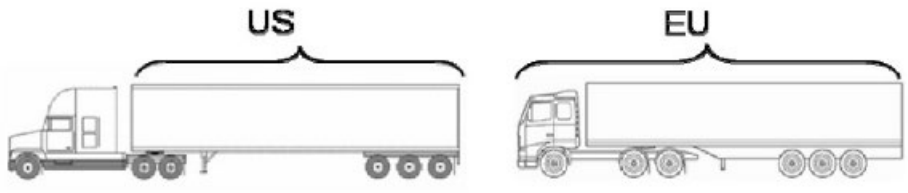


**Figure 2.1 Schematic showing the regulatory differences between the U.S. and EU length restrictions for high-sided vehicles. Reproduced from Browand et al. (2009)**

As a result of these length restrictions, in the U.S., the tractor design is such that the engine sits in front of the cab, whereas in the EU, the cab is over the engine (CoE) to utilize the maximum allowable space for the trailer. We note the CoE design is utilized in other countries outside the EU, including Australia, Mexico, and South Africa among others. As noted previously, most of the research has come from the EU and as such, aerodynamic coefficients have been primarily computed from CoE high-sided vehicles, indicating a knowledge gap for U.S. conventional high-sided vehicles.

Some simplified high-sided vehicle models have been designed to standardize analysis (Choi et al. 2014), as shown in Figure 2.2. The ground transportation system (GTS) and modified-GTS (M-GTS) are representative of the EU's CoE high-sided vehicle (Croll et al. 1995). The generic conventional model (GCM) and the modified GCM (M-GCM) are similar in style to the U.S. high-sided vehicle models (Storms et al. 2006). For the present study, we use a revised form of the GCM (Figure 2.2, lower left corner) to allow for the simplification because the high level of detail associated with M-GCM is not necessary for the purpose of this study. The trailer length is taken to be 53 feet to reflect the typical length of trailers in the U.S. with all other model dimensions consistent with typical U.S. high-sided vehicle dimensions. This particular configuration will be referred to as the 53-GCM this report.

## 2.4 Dependence of Confined Flow on Reynolds Number

The dynamics of flow around immersed (bluff) bodies under free flow conditions (i.e., away from any boundaries), e.g., flow around a cylinder, has been studied extensively. Such flows exhibit symmetry and Reynolds number independence (e.g., for the drag coefficient $C_{drag}$) as the Reynolds number increases (Gerhard et al. 2016; Yang et al. 2021). However, there are no documented studies that show such an independence for an overturning high-sided vehicle.

As shown in Figure 1.2, there is a significant spread in $C_{rolling}$ (Baker and Soper 2022) for yaw angles between 45° and 90°. Most of the studies were conducted at Reynolds numbers ranging from $8.5 \times 10^4$ to $1.25 \times 10^5$, which are too low to be fully representative of realistic conditions in which overturning crashes may occur. Regardless, most previous studies tend to conclude that the effect of Reynolds number dependency is negligible. This argument is predicated using studies of high Reynolds number crosswind interactions with railroad cars. However, it is unknown if this extrapolation to high-sided vehicles is accurate given the

significant difference in the gap ratio between the underside of the high-sided vehicle to the road compared with that of a train. Thus, it is imperative to evaluate the Reynolds numbers up to realistic high wind speeds that could cause overturning crashes.

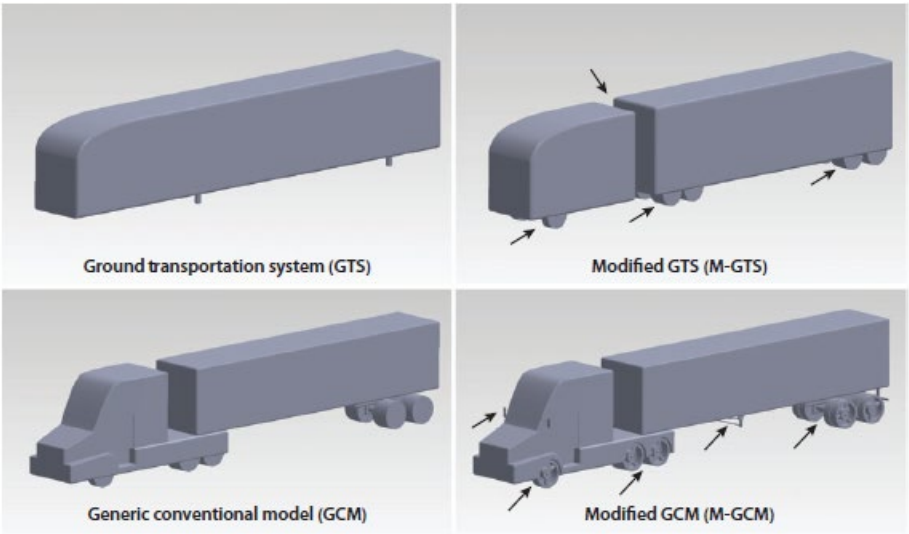


**Figure 2.2 Schematic showing the different types of simplified high-sided vehicle models. Reproduced from Choi et al. (2014)**

## 2.5 Simplification of Trailer Section into 2D Rectangular Cylinder

Given the complexity of the geometry and problem at hand, the three-dimensional problem of overturning a high-sided vehicle is simplified into flow around a rectangular cylinder near a plane wall boundary, in which the rectangular cylinder represents the trailer section of the high-sided vehicle. This simplification of the problem would allow for an investigation into the Reynolds number dependency effects (discussed in Section 2.6). This is justified given that the trailer section of a high-sided vehicle is the most prominent part of the vehicle. Therefore, the primary focus here is on conducting a high-resolution CFD simulation study using a cross section of the trailer. Hence, the configuration of a CFD model with a 2D rectangular cylinder near a plane wall boundary becomes a representative model of the problem.

There is an extensive body of work for cylinders of various shapes in free flow. In contrast, the scope of research on flow interactions with a cylinder near a plane wall boundary is limited, especially for a rectangular cylinder. For circular cylinders near a plane wall boundary, there is a dearth of studies that explore Reynolds number effects (Zdravkovich 1985; Bearman and Zdravkovich 1978; Roshko et al. 1975). Studies on rectangular cylinders near a plane wall boundary have been restricted to Reynolds numbers in the range of laminar and transition regimes with a range from 50 to 4 x $10^5$ (Bhattacharyya and Maiti 2004; Cheng et al. 2007; Mahir 2009; Yang et al. 2022; Forouzi Feshalami et al. 2022).

## 2.6 Summary

The influence of a wall boundary in proximity to the underside of a high-sided vehicle, together with the Reynolds number dependency, have received little attention in the literature. The primary question from a fundamental perspective shifts to: Is flow around a high-sided vehicle, or in general, flow around a rectangular cylinder close to a plane wall from underneath subject to Reynolds number dependency? The primary focus of this study is to explore this issue under realistic high crosswind speeds that may cause overturning.

# 3. CFD MODEL, SETUP, VERIFICATION AND VALIDATION

## 3.1 Introduction

Partially confined flow is important in engineering applications, such as the problem of this study pertaining to high-sided vehicles (known internationally as tractor-trailer vehicles, semi-trucks, or articulated lorries) overturning due to high crosswinds.

This chapter provides an overview of the computational fluid dynamics (CFD) method and tools used to investigate the flow dynamics around a rectangular cylinder near a plane wall boundary that is representative of a high-sided vehicle's trailer section. A well-constructed CFD (numerical) model includes verification and validation as key components. In CFD studies, it is best practice to perform a model verification test, typically a grid independence test, to verify that the CFD results are accurate with respect to mesh sizing (Versteeg and Malalasekera 2007). This study shows that model verification examined solely through grid independence is not adequate. A comprehensive verification study is necessary in high Reynolds incompressible flows, especially for flows around a bluff body; additional care must be taken when constructing the computational fluid flow domain and evaluating CFD results.

## 3.2 Model Parametric Framework & Numerical Methodology

The 2D cross section of the rectangular cylinder used in this study is based on a cross section of a high-sided vehicle's trailer section as shown in Figure 3.1 in free flow conditions. In Section 3.4.1, the same cross-section is used (Figure 3.3) under confined conditions near a plan wall boundary that is representative of crosswind flow over a high-sided vehicle. The model studies use Reynolds number similitude at a model scale of 1:8 (with water as the model fluid). The characteristic length scale of the model cylinder based on 53-GCM vehicle height is 0.365 m. Verification studies of the CFD model are at Reynolds numbers of $1.94 \times 10^6$ and $1.12 \times 10^7$, respectively. Validation of the CFD model uses experimental results conducted at a Reynolds number of 100,000.

### 3.2.1 Governing Equations of Motion

The governing equations of incompressible fluid flow are the Navier-Stokes (momentum) equations coupled to the conservation of mass flow equation as follows (Kundu et al. 2016):

$$\rho\left(\frac{\partial u_j}{\partial t} + u_i \frac{\partial u_j}{\partial x_i}\right) = -\frac{\partial P}{\partial x_j} + \rho g_j + \mu \frac{\partial^2 u_j}{\partial x_i^2} \tag{3.1}$$

$$\nabla \cdot \bar{u} = 0 \tag{3.2}$$

where $u_j$ is the velocity component in the direction $x_j$, and $P$ is the pressure.

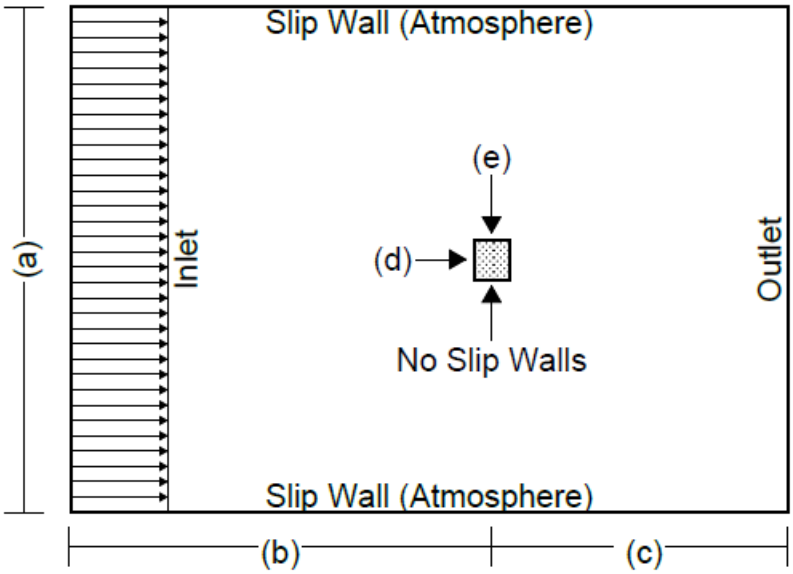


**Figure 3.1 Schematic of validation geometry depicting a rectangular cylinder in free flow**

### 3.2.2 CFD Solver – OpenFOAM

The CFD code OpenFOAM (Open-source Field Operations and Manipulations) is a set of C++ libraries solving differential equations of the flow equations using the finite-volume method for unstructured meshes (Robertson et al. 2015). It is highly parallelizable using the message passing interface (MPI). This study made use of OpenFOAM version 9. Due to the high Reynolds number involved, an unsteady flow field is expected. As such, an unsteady Reynolds-averaged Navier-Stokes (URANS) simulation was desirable. The PISO (pressure implicit with splitting of operators) method was used to facilitate URANS. Turbulence closure was achieved using the $k$-$\omega$ SST turbulence model (Menter 1994). A first-order upwind spatial scheme was implemented for all the turbulence variables. The Crank-Nicolson method was used for time discretization with a blending factor of 0.7, resulting in an approximately second-order time scheme.

The ground surface and the surface of the rectangular cylinder were specified as walls where a no-slip velocity boundary condition was imposed. At the atmospheric boundary, the free-slip condition was allowed. At the outlet, the flow was assigned a zero gradient condition. The inlet flow was specified as a zero-pressure gradient condition with a fixed value condition for the velocity with a specific dissipation rate, turbulent kinetic energy, and turbulent viscosity. Further details of the model setup are provided in Sanchez (2023).

## 3.3 Validation of Model

A validation study was done to certify the use of OpenFOAM and the model setup. Figure 3.1 shows the schematic for the flow domain used in OpenFOAM. The grid size used was 0.01 m. The flow domain was sized as follows with reference to Figure 3.1: (a) vertical domain height of 12 m, and total horizontal domain length of 17 m, with (b) 10 m upstream from the cylinder centroid, and (c) 7 m length downstream from the cylinder centroid. A rectangular cylinder, simulating the trailer section of a high-sided vehicle at $1/8^{th}$ scale, was used with (d) a cylinder height of 0.365 m, and (e) a cylinder of width of 0.324 m.

This validation study used an interpolated drag coefficient ($C_{drag}$) based on an experimental dataset utilizing rectangular cylinders with varying width to height ratios (Blevins 1984; Courchesne and Laneville 1979; Hoerner 1965). Figure 3.2 shows the data (Blevins 1984) with an interpolated target $C_{drag}$ of 2.256 highlighted by the triangle. Table 3.1 shows the measured drag coefficient from the OpenFOAM model, which is dependent on the number of inflation layers used and the percentage error relative to the interpolated drag coefficient. The error ranges from -0.742% to 6.245% but is within a reasonable limit for all cases. Based on best practices for developing a mesh with appropriate $y+$ bounds, 0 inflation layers is ideal for the validation model. For the verification geometry, 6 inflation layers were selected according to the $y+$ constraints. Note $y+$ is a nondimensional measure of wall distance units; $y+ = u_\tau y/\nu$, where $u_\tau$ is the friction velocity and $y$ is the wall normal distance (Pope 2000) In both cases, the percent error is reasonable at 6.246% and 3.529%, respectively.

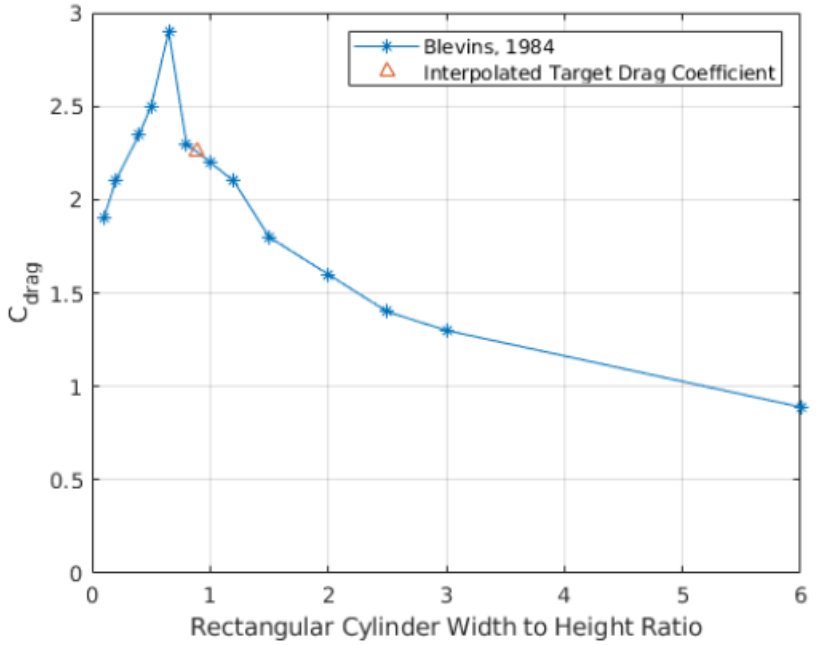


**Figure 3.2 Drag coefficient for varying rectangular cylinder width to height ratio, *Re* = 100,000**

**Table 3.1 Drag coefficient (Cdrag) for free flow analysis with varying inflation layers, Re = 100,000**

| Number of Inflation Layers | Average Drag Coefficient | Percent Error Relative to Interpolated Cd Value (%) |
|---|---|---|
| 0 | 2.397 | 6.246 |
| 2 | 2.301 | 1.974 |
| 4 | 2.239 | -0.743 |
| 6 | 2.336 | 3.529 |
| 8 | 2.198 | -2.57 |

## 3.4 Comprehensive Verification

It was found that the typical methods employed to conduct model verification are not satisfactory to ensure model accuracy. Model verification often involves refining the cell mesh and inspecting how specific quantities throughout the system may change. Once the specified quantities have stabilized with a certain grid size, the mesh is independent of the final solution. This method is adequate if, and only if, the CFD practitioner is confident that the CFD domain sizing is independent of the results.

A case for a comprehensive verification study as it pertains to 2D incompressible high Reynolds number flow around a bluff body near a plane wall boundary is presented. Because of the complex flow dynamics associated with this incompressible flow, the domain sizing is of utmost importance in tandem with a traditional grid independence analysis. Without domain size verification, errors up to 80% are possible due to improper domain sizing in any coordinate direction. Qualitative means for assessing the domain boundary sizing will be presented to allow the user to understand the flow dynamics that are influenced with each boundary.

### 3.4.1 Verification Model Geometry and Setup

The comprehensive verification domain and geometry was constructed with a rectangular cylinder at 1/8$^{th}$ scale simulating the trailer section of a high-sided vehicle near the ground surface. This rectangular cylinder was placed inside a 2D flow domain. Figure 3.3 shows a schematic for the flow domain with the key dimensions highlighted.

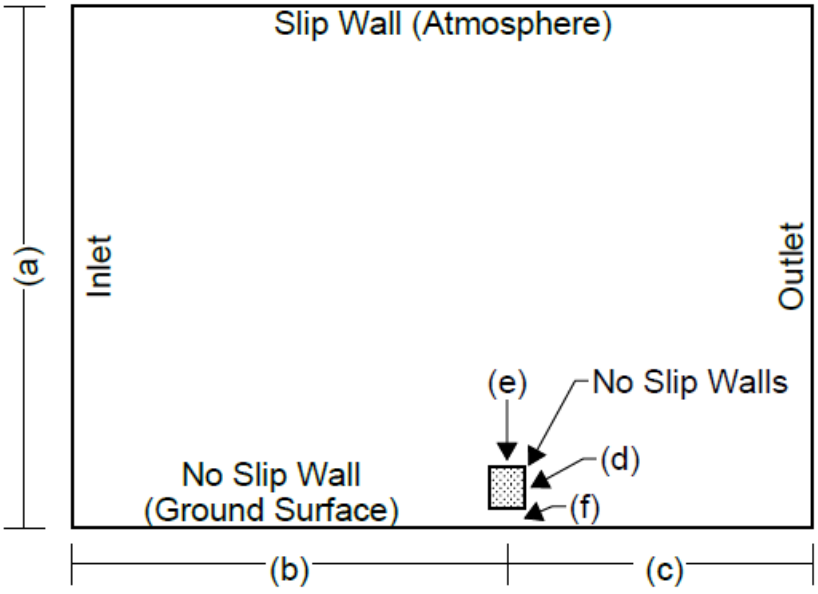


**Figure 3.3 Schematic of verification geometry depicting a rectangular cylinder near a plane wall boundary**

The parameters (a), (b), and (c) are referenced in Table 3.2 and were varied within the given bounds during the comprehensive verification study. The dimensions of the rectangular cylinder are as follows: (d) cylinder height of 0.365 m, (e) cylinder width of 0.324 m, and (f) gap height of 0.1485 m between the ground surface and bottom of the cylinder with a resulting gap ratio (gap height/cylinder height) of 0.407 (Forouz Feshalami et al. 2022). Table 3.2 provides the initial flow domain parameters, the value ranges explored for the comprehensive verification study, and the final parameters based on the comprehensive verification study

conclusion. These parameters are the focal point of the verification study and hence discussed further in what follows.

To perform the domain sizing verification, model simulations were conducted using two distinct Reynolds numbers: $1.94 \times 10^6$ and $1.12 \times 10^7$, which are one order of magnitude apart. A parametric analysis was conducted, changing the parameters of one domain boundary at a time to determine when the model was domain independent.

**Table 3.2 Parameters explored in the comprehensive verification study**

| | Initial Prescribed Value | Range Explored | Final Parameters from Comprehensive Verification Study |
|---|---|---|---|
| Number of Inflation Layers on Ground Surface | Not Prescribed | 6-10 | 10 |
| Number of Inflation Layers on Rectangular Cylinder | Not Prescribed | 0-8 | 6 |
| a) Vertical Domain Height | 2m | 2m-20m | 12m |
| b) Horizontal Domain – Length Upstream from Cylinder Centroid | 5m | 2m-20m | 10m |
| c) Horizontal Domain – Length Downstream from Cylinder Centroid | 5m or 2m | 2m-20m | 7m |
| Uniform Cell Size | 0.01m | 0.005m-0.05m | 0.01m |

### 3.4.2 Inflation Layer Selection

Given that the $k-\omega$ *SST* model was selected to resolve the Navier-Stokes equations, the inflation layers had to be refined adequately to be within the prescribed bounds necessary for using the $k-\omega$ *SST* model, as well as optimizing computational expense so extra inflation layers were not needlessly refined. $y+$ was confined to an absolute minimum of no less than 1, a preferred range of 40 to 300, with a preferred average of 150 (Menter et al. 2003).

The verification domain walls are the ground surface and the rectangular cylinder. Because these walls serve different purposes, 1) confining the flow and 2) being the bluff body study object, it was found that independent inflation layer optimization would be needed. Once the inflation layers were selected, they were kept constant to remove a variable from the following analysis. The inflation layer selection simulations used a cell size of 0.01m.

***Ground Surface Inflation Layers***

The ground surface inflation layers were checked with the flow development simulations, which are discussed in section 3.4.4. The inflation layers were varied at 6, 8, and 10, and were evaluated at the previously stated high and low Reynolds numbers with a flow development section of 100 m in length and 2 m in height. Based on this analysis, 10 ground surface inflation layers provide an adequate $y+$ range on the ground surface boundary.

***Rectangular Cylinder Inflation Layers***

The rectangular cylinder inflation layers were checked using a generic validation simulation with a 10-m vertical domain height, 5-m length upstream from the cylinder centroid, and 9-m length downstream from the cylinder centroid. In the same manner, this simulation was evaluated at the high and low Reynolds numbers. Based on this analysis, six rectangular cylinder inflation layers provide the optimal means to stay within the prescribed $y+$ boundaries.

### 3.4.3 Vertical Domain Height

The study first focused on the vertical domain size. To speed up the computational process, a uniform flow profile was chosen, as the type of flow (uniform versus developed) is a secondary factor relative to the vertical domain height. Since the horizontal domain size had not yet been explored, a domain length of 7 m was arbitrarily selected, with 5 m upstream and 2 m downstream from the cylinder's centroid. The vertical domain height was varied between 2 m and 20 m. Figure 3.4 (upper panel) displays the resulting average drag coefficient on the body, while Figure 3.4 (lower panel) shows the percentage error relative to the minimum value for each Reynolds number (at 12 m for each Reynolds number). A qualitative analysis of Figure 3.4 (upper panel) indicates that a minimum vertical domain height of 8 m is necessary for either Reynolds number. Furthermore, Figure 3.4 (lower panel) quantitatively demonstrates that the drag coefficient becomes independent of vertical domain height beyond 12 m.

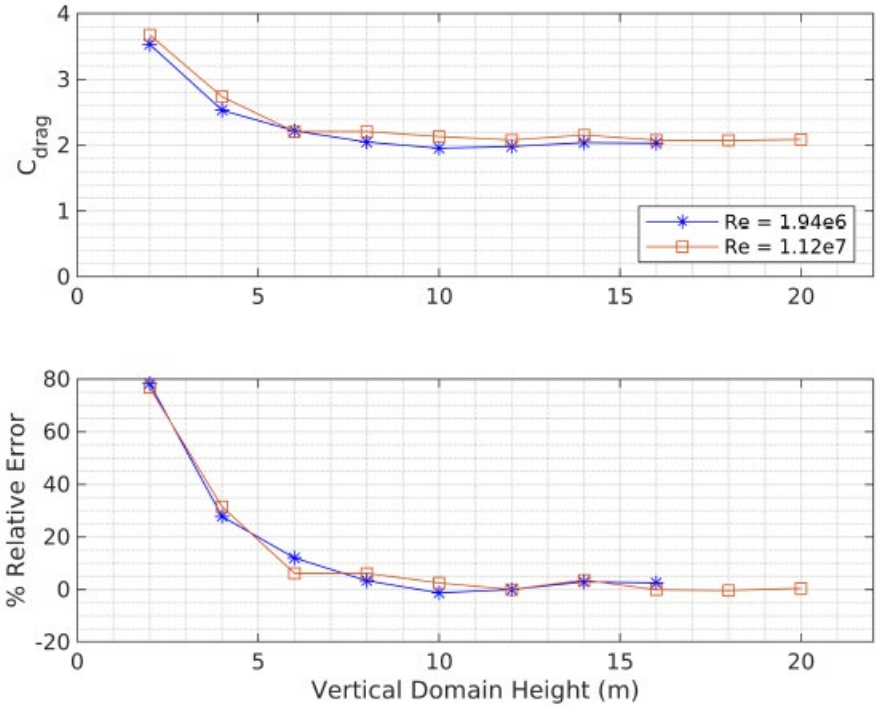


**Figure 3.4 Comprehensive verification study to investigate the vertical domain height of the model: (upper panel) drag coefficient versus vertical domain height; (lower panel) percent error relative to selected converged value at 12 m**

Figure 3.5 illustrates the difference in instantaneous flow structures between vertical domain heights of 2 m and 12 m. It shows that the streamlines are compressed in the 2-m domain (left panel), resulting in increased velocity, as indicated by the higher velocity regions in the figure. This localized acceleration artificially raises the drag coefficient experienced by the body.

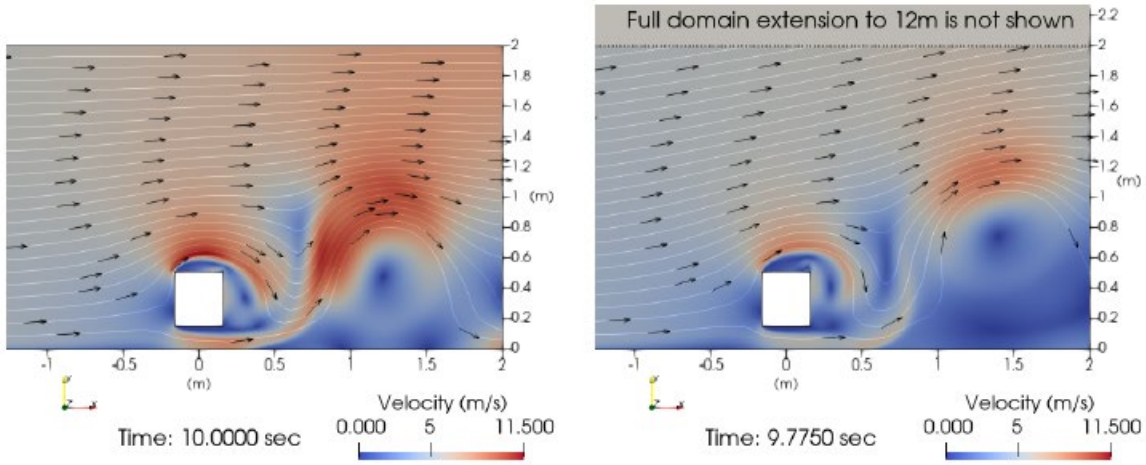


**Figure 3.5 Flow fields for a domain height of 2 m (left panel) versus 12 m (right panel) at a Reynolds number Re=1.94 x 106**

### 3.4.4 Developed Flow Profile

To streamline the repetitive parametric foundation of the comprehensive verification study, a developed flow profile was created using the selected vertical domain height of 12 m. This developed flow profile was then used as input for the subsequent models. Figure 3.6 illustrates this profile, generated over a 100-m-long section with a height of 12 m, starting with a uniform flow profile at the inlet. The developed flow profile was extracted at the outlet once the developed layer reached approximately 0.6 m, which was sufficient to fully encompass the height of the rectangular cylinder.

Figure 3.7 illustrates a developing flow profile with a height of up to 0.6 m, which is adequate to cover the entire rectangular cylinder. The flow was not extended to cover the full 12-m domain because the computational cost grows exponentially with the length required to increase the developed flow height. For instance, a 200-m section is needed to achieve a developed flow height of 0.8 m, but this additional 0.2 m would take roughly twice as long to compute compared with the 100-m section required for the original flow development.

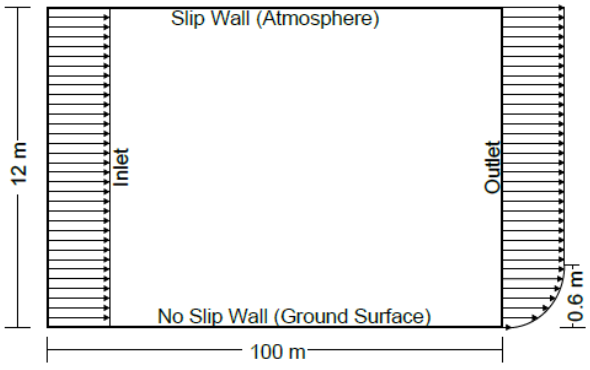


**Figure 3.6 Developed flow profile at outlet of a 100-m section with uniform inflow**

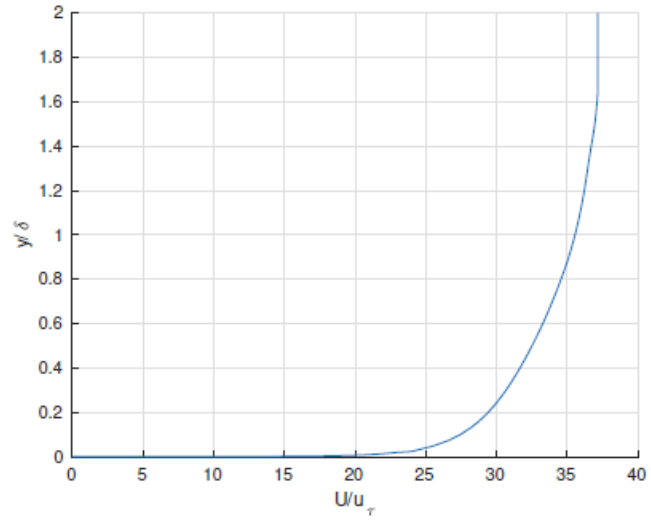


**Figure 3.7 Non-dimensional plot of developed flow profile, where $\delta$ is the rectangular cylinder height and $u_\tau$ is the friction velocity**

### 3.4.5 Horizontal Domain: Length Upstream from Cylinder

The investigation of the horizontal domain began with the length upstream of the cylinder's centroid. As previously noted, a developed flow profile was utilized for this analysis. The length downstream from the cylinder centroid was fixed at an arbitrary 5 m, while the upstream length varied from 2 m to 20 m. Figure 3.8 (upper panel) shows the resulting average drag coefficient experienced by the body. Figure 3.8 (lower panel) shows the percent error relative to the average drag coefficient for the selected upstream length (at 10 m for each Reynolds number).

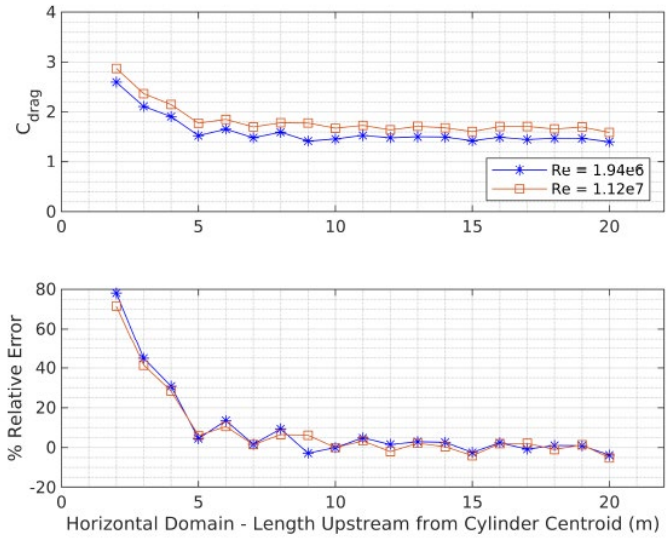


**Figure 3.8 Comprehensive verification study to investigate the horizontal domain length upstream from cylinder: (upper panel) drag coefficient versus horizontal domain length; (lower panel) percent error relative to selected converged value at 10 m**

These results reveal an oscillatory pattern that gradually stabilizes around an average value. A length of 10 m was chosen for both datasets because it occurs after the oscillations have diminished, and it represents the average value that the system converges toward as the parametric analysis extends beyond 10 m. Figure 3.8 (lower panel) illustrates that the data converge, indicating consistent behavior in response to variations in upstream length.

Alongside the quantitative methods, a qualitative approach was employed to estimate the necessary horizontal domain length upstream of the cylinder's centroid. Figure 3.9 presents the results of a simulation with a 20-m horizontal domain length upstream from the cylinder centroid, showing a pressure plot extending from the stagnation point on the centroid of the rectangular cylinder's inlet face to the inlet boundary. The 20-m length was selected arbitrarily, assuming it would be sufficient to encompass the final required domain length. The pressure graph suggests that approximately 8 m are needed for the stagnation pressure effects to dissipate before reaching the inlet boundary. Figure 3.9 qualitatively supports the quantitative findings presented in Figure 3.8.

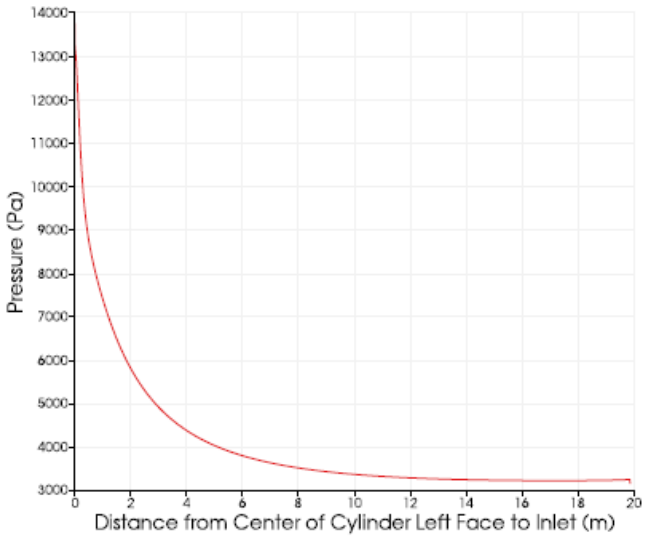


**Figure 3.9 Average pressure along the streamline connecting the stagnation point on the rectangular cylinder to the inlet, Reynolds number $Re = 1.94 \times 10^6$**

### 3.4.6 Horizontal Domain: Length Downstream from Cylinder

The final component of the horizontal domain investigated was the length downstream from the cylinder centroid. A developed flow profile was employed for this analysis. The length upstream from the cylinder centroid was fixed at 5 m, while the downstream length was varied between 2 m and 20 m. Figure 3.10 (upper panel) displays the average drag coefficient experienced by the body, while Figure 3.10 (lower panel) illustrates the percent error relative to the average drag coefficient for each downstream length, with the reference being 7 m for each Reynolds number.

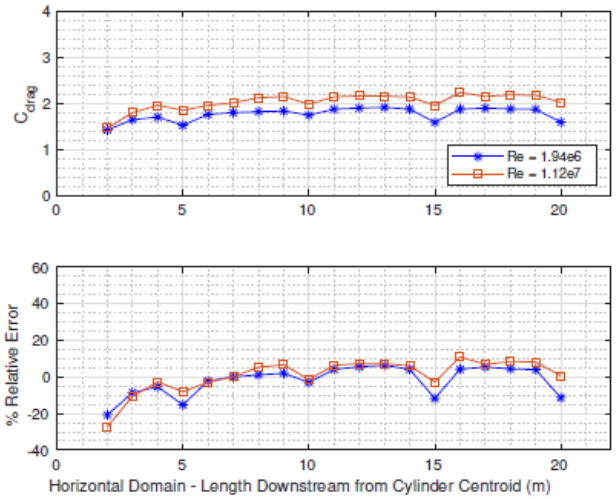


**Figure 3.10 Comprehensive verification study to investigate the horizontal domain length downstream from cylinder: (upper panel) drag coefficient versus horizontal domain length; (lower panel) percent error relative to selected converged value at 7 m**

There was not an explicit trend to identify a specific length, but best practices in wind tunnel experiments recommend that the minimum downstream length should be sufficient for the wake to fully expand before leaving the tunnel (Rae et al. 1999). Following this guideline, a length of 7 m was chosen because, as shown in Figure 3.11, the wake width is maximized at this distance, and the flow exits the simulation with nearly horizontal velocity.

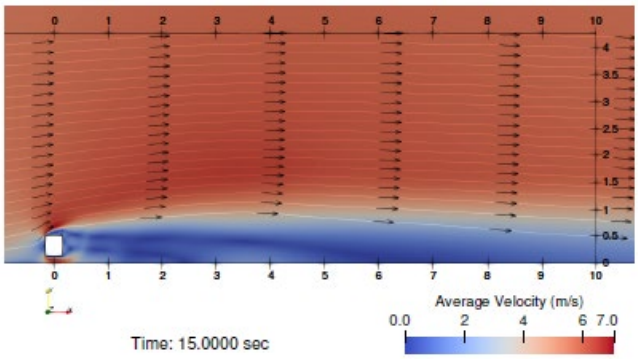


**Figure 3.11 Average velocity with streamlines superposed. The flow at 7 m is where the wake is at its largest width and the velocity vector is approximately horizontal, Reynolds number *Re* = 1.94 x $10^6$**

### 3.4.7 Traditional Grid Refinement Independence

After finalizing the domain parameters, a grid refinement check was conducted. Figure 3.12 demonstrates that a mesh with approximately 2 x $10^6$ cells is sufficient, corresponding to a standard cell size of 0.01 m. Consequently, the previous results are independent of grid size.

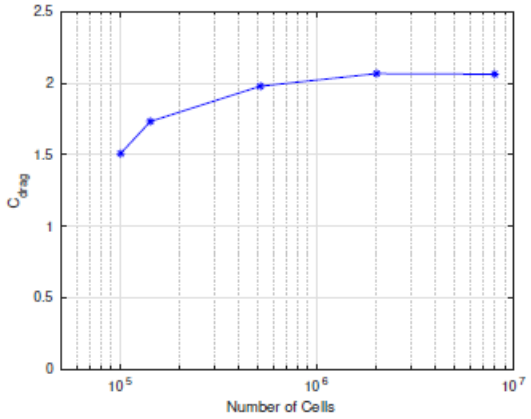


**Figure 3.12 Traditional grid refinement, Reynolds number *Re* = 1.94 x $10^6$**

### 3.4.8 Discussion of Comprehensive Verification Study Results

Based on this analysis, the final domain parameters listed in Table 3.2 were chosen. The value of conducting a thorough verification study is highlighted by the error graphs. Figure 3.4 (lower panel) indicates an 80% error for a 2-m vertical domain height, which reduces to 10% with a 6-m height. Figure 3.8 (lower panel) shows a 70% error for a 2-m length upstream from the cylinder centroid. Additionally, Figure 3.10 (lower panel) reveals an underprediction error of about -20% for a 2-m length downstream from the cylinder centroid. These errors arise due to the following reasons:

- If the vertical domain height is too small, the streamlines become compressed, as illustrated in Figure 3.5.
- If the length upstream from the cylinder centroid is too short, the stagnation pressure effect is constrained and does not have enough space to fully develop, as depicted in Figure 3.9.
- If the length downstream from the cylinder centroid is too short, the development of flow features is restricted, preventing the flow wake from expanding to its maximum size, as shown in Figure 3.11

It is crucial to recognize these effects, especially for high Reynolds number flows, as an incorrectly sized flow domain can substantially distort the simulation results.

## 3.5 Recommendations and Conclusion

Throughout the validation and comprehensive verification study, recommendations were made to streamline future comprehensive verification efforts and ensure the accuracy of results. Initially, a validation study was conducted with generic domain sizing. After determining the final domain dimensions in the comprehensive verification study, the domain size from the initial validation was updated, and the validation study was rerun to align with the updated domain boundaries.

A qualitative approach is needed to determine the appropriate domain size. Figures 3.5, 3.9, and 3.11 illustrate different methods for assessing domain size effectiveness by simulating larger-than-required domain boundaries. After obtaining qualitative estimates of the domain boundaries, a comprehensive verification study should be conducted. To expedite such a study, it might be helpful to vary the domain size around the qualitative estimates to quickly converge on model behavior. Additionally, analysis of the data to produce plots similar to those in Figures 3.4, 3.8, and 3.10 would expedite the process. It is recommended to begin with larger increments, such as 5 m, and then refine the increments to 2 m, and finally 1 m, as the overall trends in the model behavior become clearer.

A case for conducting a comprehensive verification study on 2D incompressible high Reynolds number flow around a bluff body near a plane wall boundary has been outlined. Given the complexity of the flow dynamics in this incompressible flow scenario, domain sizing is crucial, alongside traditional grid independence analysis. Without proper domain size verification, errors of up to 80% can occur due to incorrect domain sizing in any direction. Qualitative methods for assessing domain boundary sizing are provided for two main purposes: 1) to help users understand how flow dynamics are influenced by each boundary, and 2) to offer an initial estimate for the required domain boundary sizing in new CFD models.

# 4. MODELING HIGH REYNOLDS FLOW AROUND RECTANGULAR CYLINDER NEAR A PLANE WALL WITH APPLICATION TO OVERTURNING HIGH-SIDED VEHICLES

## 4.1 Introduction

Flow around bluff bodies has long been a focal point in fluid mechanics, particularly with our ongoing interest in von Kármán type flow structures. However, the flow around a rectangular cylinder near a planar wall boundary remains less explored. This study addresses two notable gaps in knowledge: one in the fundamental study of fluid dynamics and another in its practical applications.

In the fundamental domain, existing research on incompressible flow around rectangular cylinders near a plane wall boundary has been limited to Reynolds numbers ranging from 50 to 4.12 x $10^5$, covering the laminar and transitional regimes (Bhattacharyya and Maiti 2004; Cheng et al. 2007; Mahir 2009; Yang et al. 2021, 2022; Forouzi Feshalami et al. 2022). This study extends beyond these ranges, exploring high Reynolds number incompressible flow up to $10^8$, thereby addressing a significant gap in the literature.

The study of overturning high-sided vehicles has been generalized to align with research on high Reynolds number incompressible flow around a rectangular cylinder near a planar wall boundary. This generalization involves examining the trailer section of a high-sided vehicle and approximating it as a 2D cross-section. This simplification will illustrate how flow characteristics depend on the Reynolds number when the rectangular cylinder is near a plane wall boundary, in contrast to a rectangular cylinder in free flow.

This chapter is organized as follows: Section 4.2 presents a nondimensional analysis and a brief overview of the comprehensive verification and validation analysis conducted as presented in Chapter 3. Section 4.3 details the results and provides a discussion. Section 4.4 provides the study's conclusions.

## 4.2 Theory, Methods, and Model Setup

### 4.2.1 Non-dimensional Analysis

A non-dimensional analysis was performed using the Buckingham pi theorem. Figure 4.1 identifies some of the system variables. These variables have been stated in their base dimensions using the basic dimensions of mass (M), length (L), and time (T). First, the dimensions of length [$L$], width [$W$], and height [$H$] are represented using the basic dimension (L). Additional variables include the relative wind velocity [$V$ ] = L $T^{-1}$, the relative wind direction (with respect to the vehicle length axis) [$\psi$] = 1, the density of air [$\rho$] = $ML^{-3}$, the dynamic viscosity of air [$\mu$] = $ML^{-1}T^{-1}$, pressure [$P$] = $ML^{-1}T^{-2}$, and the shedding frequency [$\omega$] = $T^{-1}$. There are seven distinct variables based on the identification of the unit combinations (i.e., length, width, and height function as a single variable with respect to a unit perspective). This results in four expected Π terms (seven variables minus three base dimensions).

Scaling variables are used to define the Π term. It was determined that the basic dimensions M, L, and T would be scaled as follows: L = [$H$], T = [$H/V$ ], and M = $\rho H^3$. Using these scaling variable definitions, the Π terms were defined as: [$\psi$] = 1, [$\mu$] = $\rho HV$ where Re = $\rho HV/\mu$, [$P$]= $\rho V^2$ where $Eu$ = P/ ($\rho V^2$), and [$\omega$] = $V/H$ where $St = \omega H/V$. The resulting non-dimensional grouping can be expressed as:

$$Eu = f(Re, St, \varphi) \tag{4.1}$$

The Euler number (*Eu*) serves as a general form of aerodynamic coefficients. In a direct crosswind scenario, where $\psi$ remains constant, the analysis focuses on the relationship between the Euler number, Reynolds number (*Re*), and Strouhal number (*St*). This study examines how the aerodynamic coefficients (Euler number) vary with the Reynolds number. The Strouhal number provides a measure nondimensional characteristic frequency of oscillation in the wake of the flow past the object. While the Strouhal number is also assessed in relation to the Reynolds number, its variation was found to be minimal. Given that the Euler number is a general form of aerodynamic coefficients, the specific aerodynamic coefficients ($C_{drag}$, $C_{side}$, $C_{lift}$, $C_{rolling}$), as shown in equations (2.1–2.4), can be defined (Blevins 1984) and will not be repeated here for brevity.

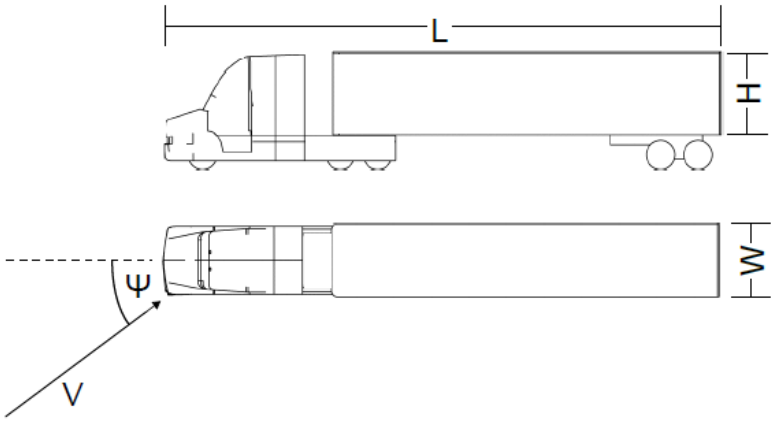


**Figure 4.1 Schematic showing key variables identified for non-dimensional analysis using pi theorem**

### 4.2.2 Model Parametric Framework

The 3D model depicted in Figure 4.1 has been simplified to a rectangular cylinder situated near a planar wall boundary, as shown in Figure 4.2. This simplified model represents the trailer section of a high-sided vehicle, with the characteristic length scale being the height of the rectangular cylinder (0.365 m) at a model scale of 1/8. Further details are provided in the following section.

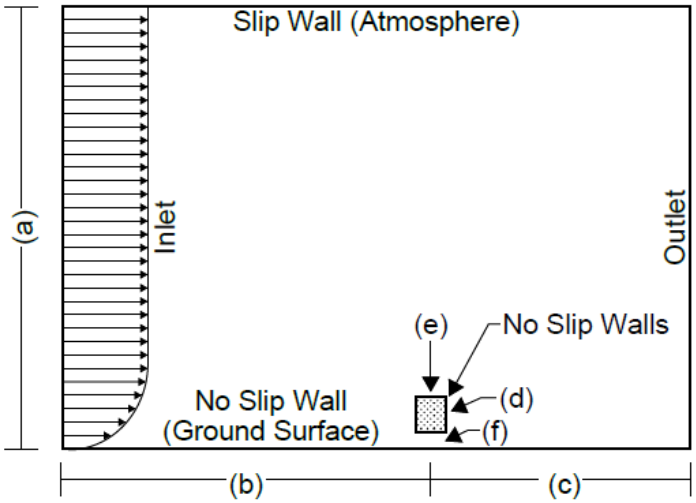


**Figure 4.2 Rectangular cylinder near a plane wall boundary with a developed inlet flow profile**

The CFD model was verified at Reynolds numbers of $1.94 \times 10^6$ and $1.12 \times 10^7$ and validated with a Reynolds number of 100,000 (see Chapter 3). This study evaluated Reynolds numbers ranging from $10^4$ to $10^8$. This range encompasses the Reynolds numbers studied in the fundamental research field (from 50 to $4.12 \times 10^5$), fully covers the Reynolds numbers examined in existing application research (from $8.5 \times 10^4$ to $1.25 \times 10^5$), and includes values relevant to realistic wind speeds where overturning crashes might occur (between $1.94 \times 10^6$ and $1.12 \times 10^7$).

### 4.2.3 Verification and Validation

A review of CFD studies on the overturning of high-sided vehicles revealed a lack of rigorous and comprehensive numerical analysis, leaving the accuracy and realism of the results uncertain (Grm and Batista 2017; Salati et al. 2018; Tunay et al. 2020; Zhang et al. 2020). This section provides the relevant details and findings from the thorough verification and validation analysis, with more information available in Chapter 3.

Initial validation of OpenFOAM was performed (as discussed extensively in Chapter 3 of this report). It was concluded that OpenFOAM produces realistic results with an error margin of approximately 7%. This validation provided confidence in the OpenFOAM model setup and confirmed that the comprehensive verification analysis and subsequent study could proceed. The comprehensive verification analysis was deemed necessary because a traditional grid independence study alone was insufficient. This thorough verification involved assessing domain sizing until flow characteristics were found to be independent of domain size. A traditional grid independence study was then conducted to complete the comprehensive verification process.

### 4.2.4 Model Setup

Based on the results presented in Chapter 3 and illustrated in Figure 4.2, the final dimensions for the rectangular cylinder in free flow and near a planar wall boundary are as follows: (a) a vertical domain height of 12 m; (b) a horizontal domain length of 10 m upstream from the cylinder centroid; (c) a horizontal domain length of 7 m downstream from the cylinder centroid; (d) a cylinder height of 0.365 m; (e) a cylinder width of 0.324 m, yielding a width-to-height ratio of 0.887; and (f) a gap height of 0.1485 m between the ground surface and the bottom of the cylinder, resulting in a gap ratio (gap height/cylinder height) of 0.407 (Forouzi Feshalami et al. 2022). A cell size of 0.01 m was utilized, as determined by the grid independence study.

The number of inflation layers required on each wall surface depended on the Reynolds number and was assessed by measuring $y^+$. The $y^+$ value was kept at a minimum of 1, with a preferred range of 40 to 300 and an ideal average of 150 (Menter et al. 2003). This approach allowed some flexibility in determining the number of layers for different Reynolds number ranges. For Reynolds numbers between $10^4$ and $7 \times 10^4$, no inflation layers were applied. For Reynolds numbers between $10^5$ and $1.12 \times 10^7$, six inflation layers were used on the rectangular cylinder surface and 10 on the ground surface. For a Reynolds number of $10^8$, 20 inflation layers were applied to the rectangular cylinder surface and 24 to the ground surface.

## 4.3 Results and Discussion

The literature often indicates that the drag coefficient is generally independent of Reynolds number. However, this study examines high Reynolds number flow around a rectangular cylinder near a plane wall boundary, as illustrated in Figure 4.2. The study evaluates Reynolds numbers ranging from $10^4$ to $10^7$. It will be demonstrated that the flow characteristics around a rectangular cylinder near a plane wall boundary depend on Reynolds number and result in an asymmetric wake, whereas flow around a rectangular cylinder in free flow shows no dependence on Reynolds number and produces a symmetric wake. Consequently, the rolling moment coefficient ($C_{rolling}$)) is influenced by Reynolds number.

### 4.3.1 Symmetric and Asymmetric Flow Structures

Figures 4.3 and 4.4 show the time signature for the drag coefficient ($C_{drag}$) for flow around a rectangular cylinder near a plane wall boundary and in free flow, respectively; this is plotted against time for Reynolds numbers 2.5 x $10^4$, $10^5$, 1.94 x $10^6$, and 1.12 x $10^7$, respectively. When comparing the graphs in Figures 4.3 and 4.4, both show cyclical patterns with peaks and valleys. However, the time signature dynamics are less pronounced in the flow around a rectangular cylinder near a plane wall boundary (Figure 4.3), whereas they are more dynamic for a rectangular cylinder in free flow (Figure 4.4). This indicates that the presence of the ground surface significantly dampens the oscillations in the flow field.

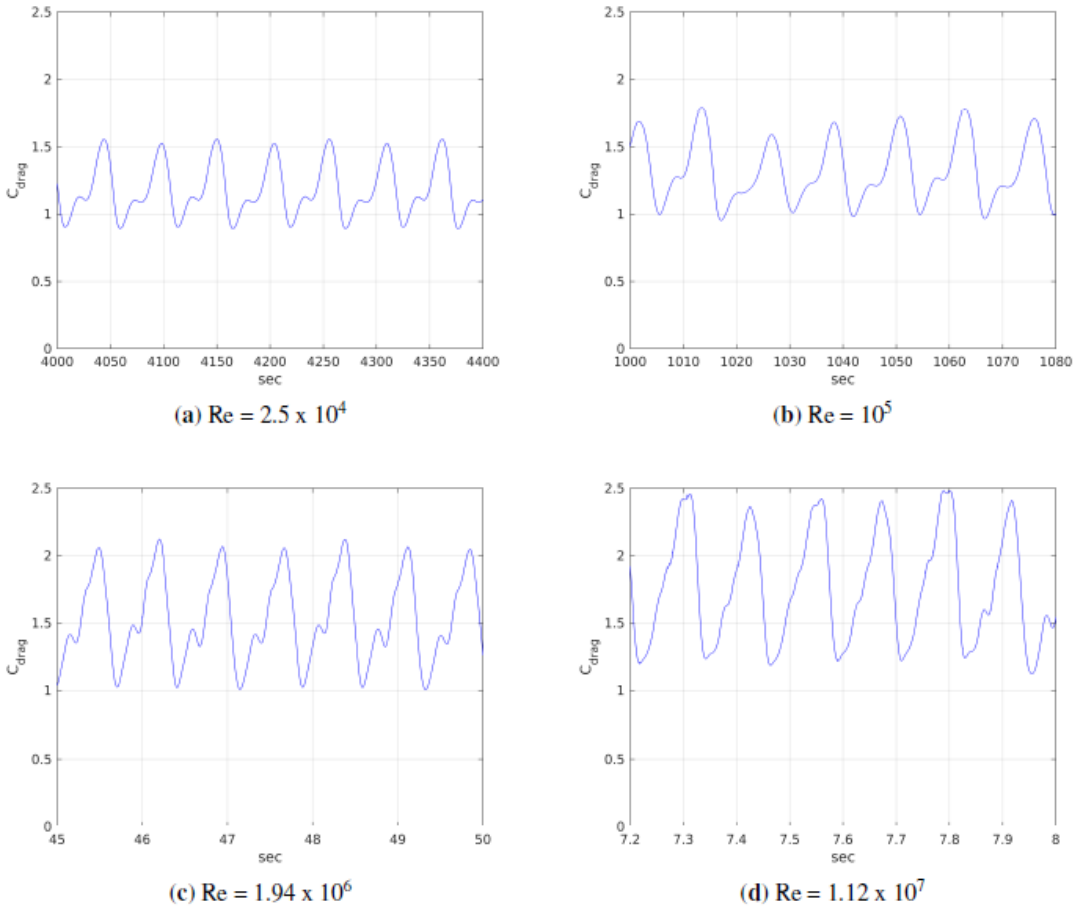


**Figure 4.3 Time signature for $C_{drag}$ for flow around a rectangular cylinder near a plane wall boundary, at Reynolds numbers of (a) 2.5 x $10^4$, (b)$10^5$, (c) 1.94 x $10^6$, and (d) 1.12 x $10^7$**

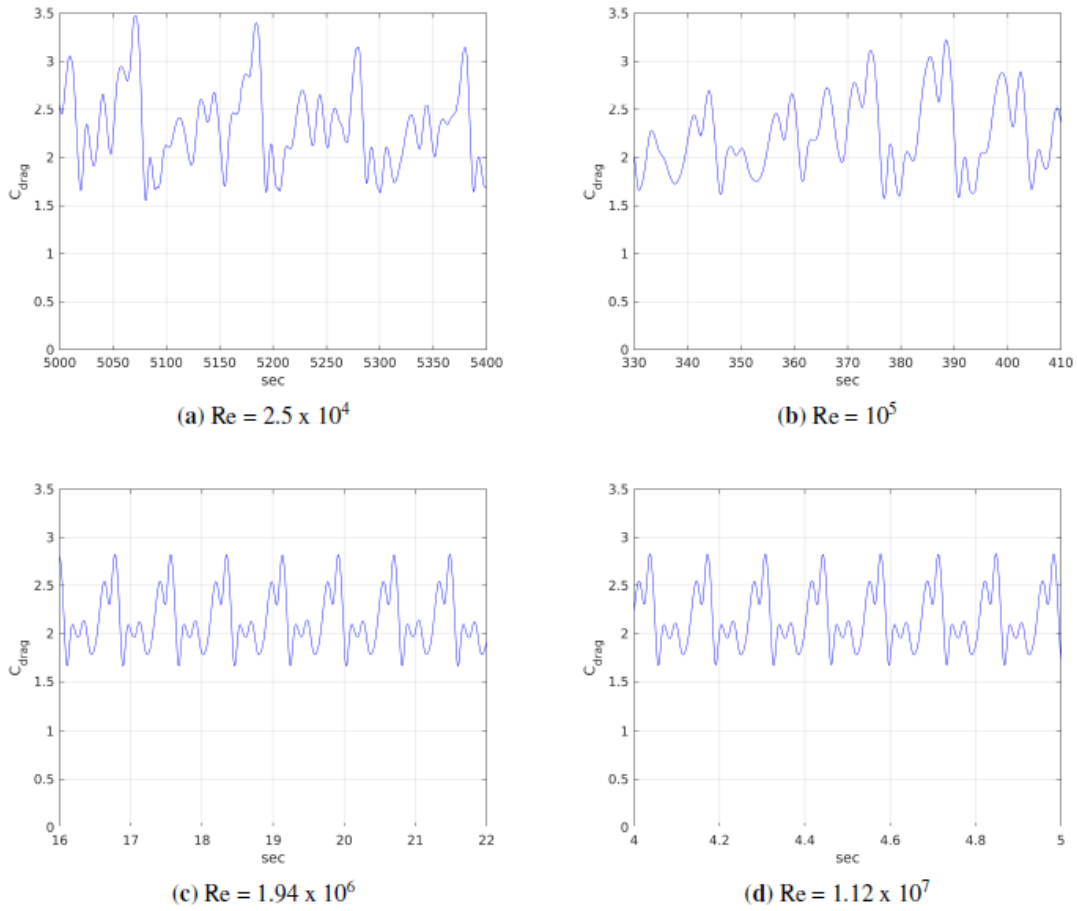


**Figure 4.4 Time signature for $C_{drag}$ for flow around a rectangular cylinder in free flow, at Reynolds numbers of (a) 2.5 x $10^4$, (b)$10^5$, (c) 1.94 x $10^6$, and (d) 1.12 x $10^7$**

The following analysis graphically examines the flow field at various timesteps, correlating flow field snapshots with corresponding points on the $C_{drag}$ plots. Figures 4.5 and 4.6 depict the oscillatory von Kármán vortex behavior in the flow around a rectangular cylinder near a plane wall boundary at Reynolds numbers of 1.94 x $10^6$ and 1.12 x $10^7$, respectively. These figures show the instantaneous URANS velocity field, with blue representing low-velocity flow and red indicating high-velocity flow. The streamlines are shown in white and the Q-criterion, set at a value of 0.5, is depicted in black. The Q-criterion, which is the second invariant of the velocity gradient tensor, identifies vortices as regions where vorticity magnitude exceeds the magnitude of the rate of strain (Zhan et al., 2019).

In Figures 4.5 and 4.6, each image iteration shows the flow progressing through its oscillatory state. Image (a) highlights accelerated flow in the gap between the rectangular cylinder and the ground surface, corresponding to the peak of the $C_{drag}$ time history. Image (b) shows the accelerated flow jetting up on the backside of the rectangular cylinder, correlating with the midpoint of the descending limb of the $C_{drag}$ time history. Image (c) shows the accelerated flow impacting the top face of the rectangular cylinder, corresponding to the $C_{drag}$ trough. Finally, image (d) depicts the underflow from the beginning of the cycle detaching from the cylinder and propagating along the ground surface, correlating with the midpoint of the rising limb.

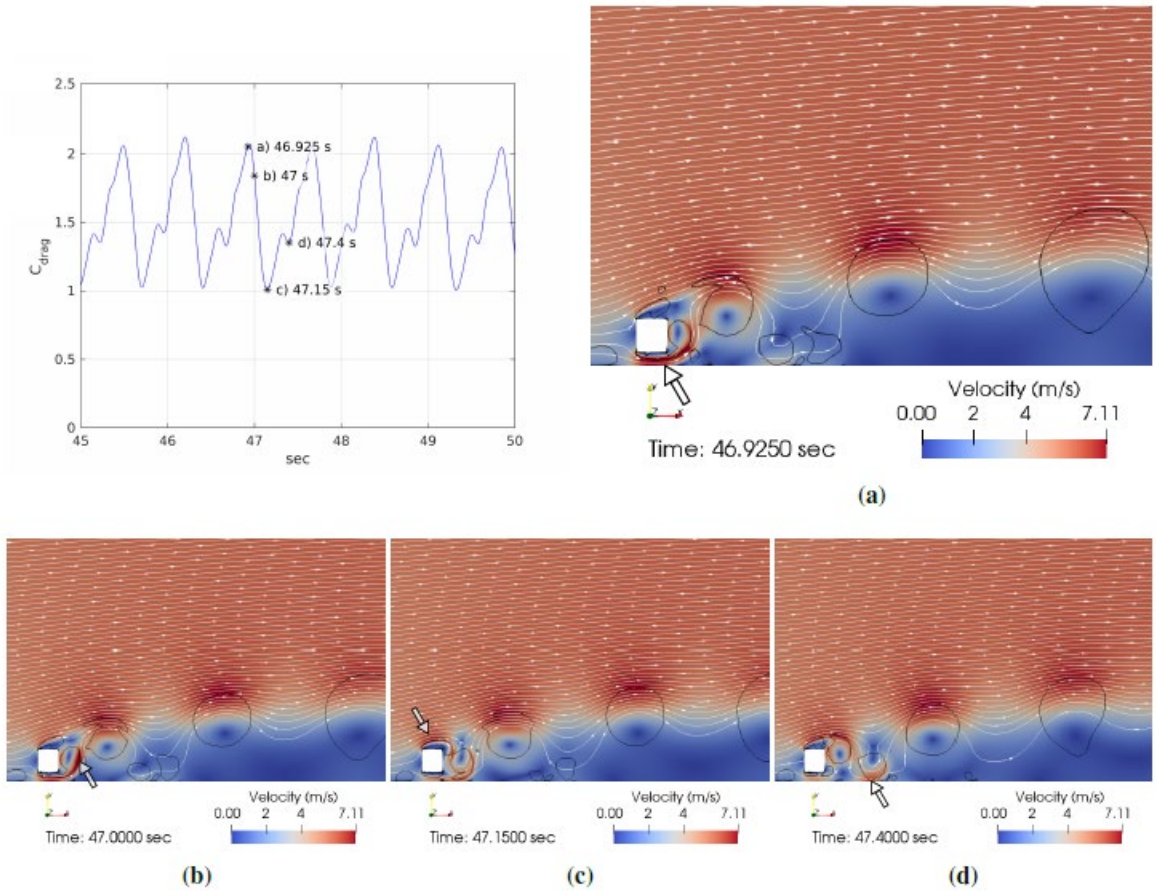


**Figure 4.5 A sequence of images showing the oscillatory and asymmetric nature of flow around a rectangular cylinder near a plane wall boundary, at a Reynolds number of 1.94 x $10^6$**

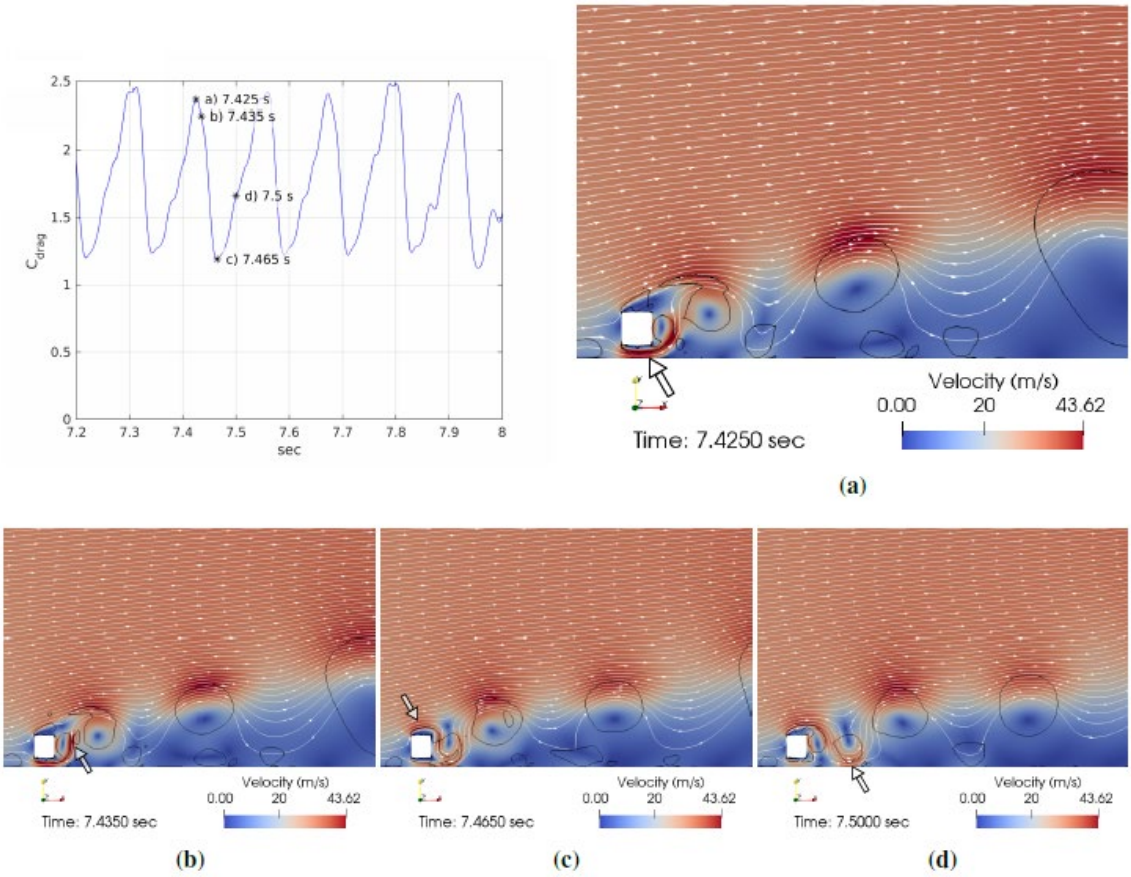


**Figure 4.6 A sequence of images showing the oscillatory and asymmetric nature of flow around a rectangular cylinder near a plane wall boundary, at a Reynolds number of 1.12 x $10^7$**

In Figures 4.7 and 4.8, each image captures the flow progressing through an oscillatory cycle, similar to the behavior shown in Figures 4.5 and 4.6 but for a rectangular cylinder in free flow. Image (a) shows the flow accelerating over the top of the cylinder, corresponding to the peak in $C_{drag}$. Image (b) captures the high flow rate switching toward the bottom of the cylinder, correlating with the trough in $C_{drag}$. Image (c) shows the accelerated flow concentrated at the bottom of the cylinder, with a slight recovery in $C_{drag}$. Image (d) shows again the flow accelerating over the top of the cylinder, where $C_{drag}$ has moderately recovered. Finally, image (e) shows the start of a new oscillatory cycle, with the accelerated flow now mirrored and concentrated at the bottom of the rectangular cylinder.

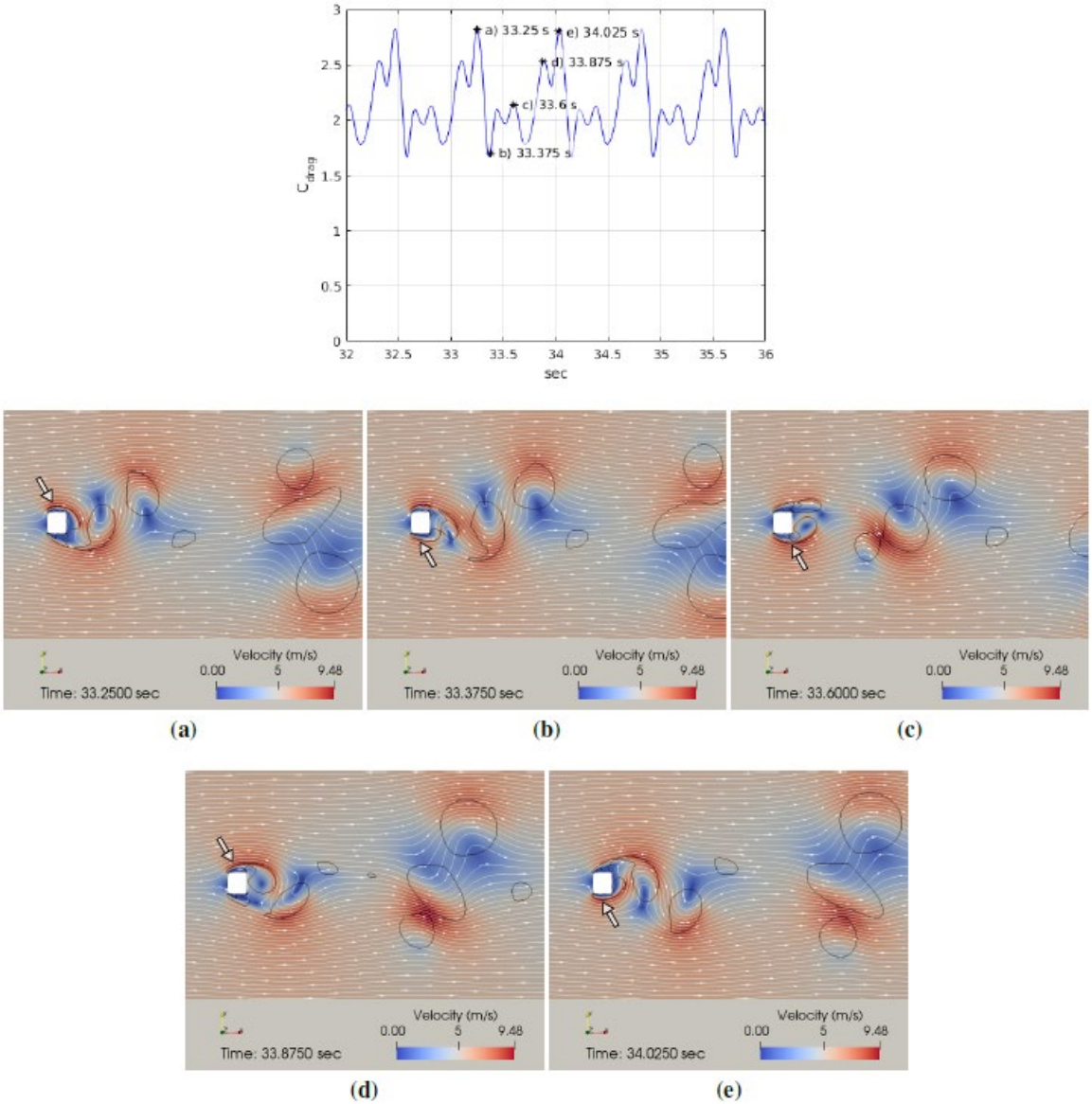


**Figure 4.7 A sequence of images showing the oscillatory and symmetric nature of flow around a rectangular cylinder in free flow, at a Reynolds number of 1.94 x $10^6$**

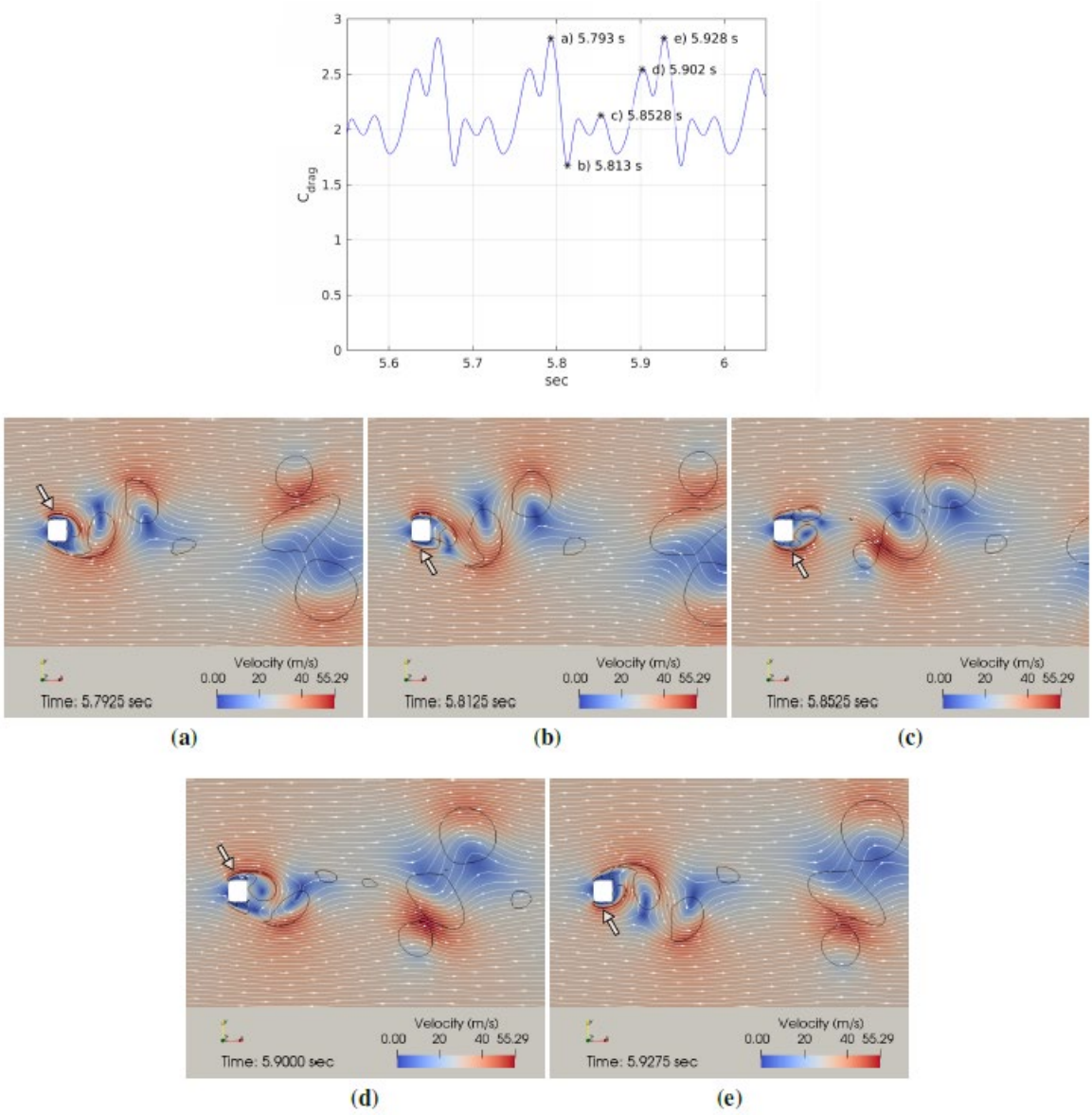


**Figure 4.8 A sequence of images showing the oscillatory and symmetric nature of flow around a rectangular cylinder in free flow, at a Reynolds number of 1.12 x $10^7$**

Figures 4.9 and 4.10 depict the average velocity fields. A comparison of these figures shows a clear difference between the asymmetric wake observed near a plane wall boundary and the symmetric wake in free flow. Figure 4.9 also shows the high-velocity jets that were highlighted in Figures 4.5b and 4.6b. Qualitatively, the flow around a rectangular cylinder near a plane wall boundary is asymmetric, while the flow around a rectangular cylinder in free flow is symmetric.

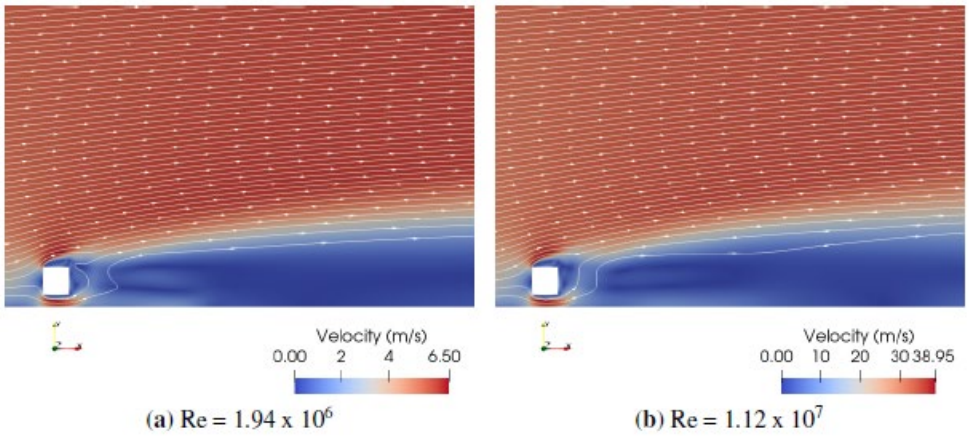


**Figure 4.9 The asymmetric average velocity field around a rectangular cylinder near a plane wall boundary**

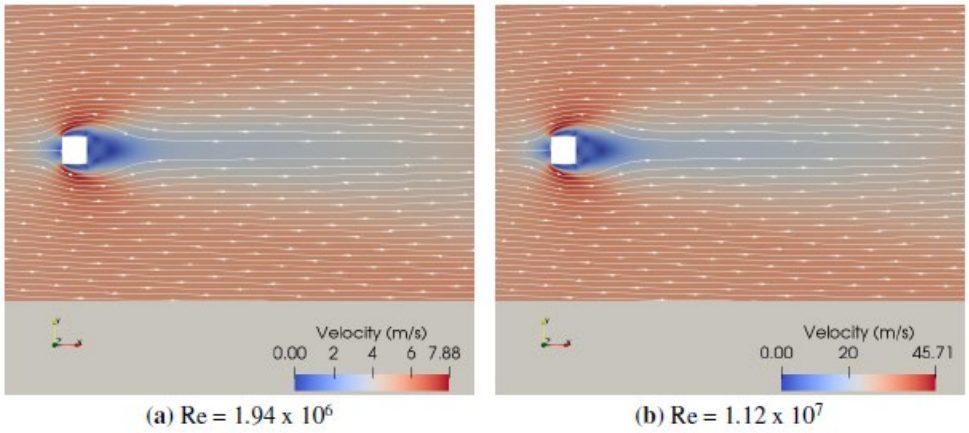


**Figure 4.10 The symmetric average velocity field for flow around a rectangular cylinder in free flow**

### 4.3.2 Aerodynamic Coefficients

The main focus of this study is to demonstrate that the flow characteristics around a rectangular cylinder near a plane wall boundary are dependent on the Reynolds number, up to at least 1.12 x $10^7$. Figure 4.11 shows the drag coefficient ($C_{drag}$) on the rectangular cylinder for both (a) flow near a plane wall boundary and (b) free flow. It is apparent that the flow around a rectangular cylinder near a plane wall boundary is influenced by the Reynolds number, as indicated by Equation (4.1).

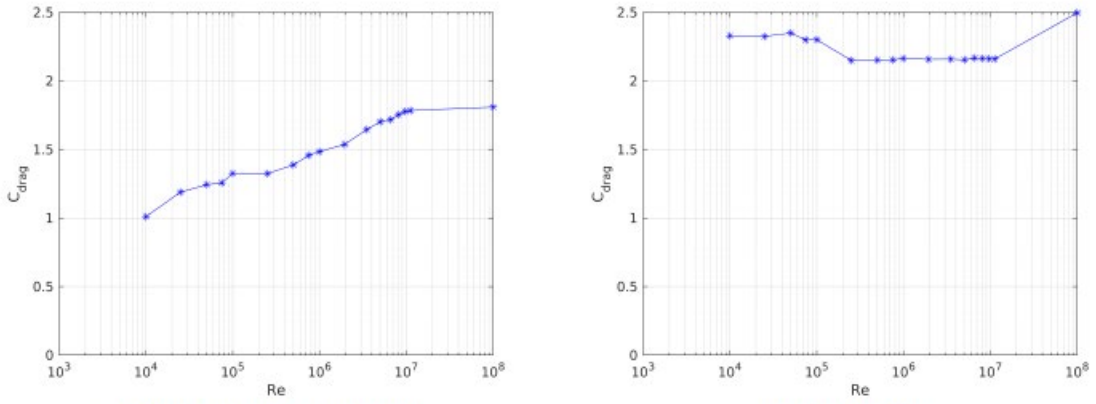


**Figure 4.11 $C_{drag}$ measured for flow around a rectangular cylinder (a) near a plane wall boundary and (b) in free flow**

Figure 4.11a shows a significant dependence of the drag coefficient ($C_{drag}$) on the Reynolds number for all values up to 1.12 x $10^7$. For the single analysis conducted at a Reynolds number of $10^8$, $C_{drag}$ appears to approach Reynolds number independence. However, additional simulations are needed to confirm this observed Reynolds number independence at values exceeding 1.12 x $10^7$.

Figure 4.11b is compared with traditional drag coefficient ($C_{drag}$) literature (Blevins 1984), which indicates that for a circular cylinder, $C_{drag}$ becomes independent of Reynolds number above approximately 1,000 but experiences a drag crisis around a Reynolds number of 5 x $10^5$ before recovering above $10^6$. A notable difference is that the asymptotic $C_{drag}$ values are distinct: an average of 2.22 for the rectangular cylinder compared with approximately 1.2 for the circular cylinder. Although $C_{drag}$ is known to depend on the shape of the object (Blevins 1984), the asymptotic behavior is observed for both cylinder shapes in free flow.

Figures 4.12 and 4.13 show the variation of the side coefficient ($C_{side}$) and the lift coefficient ($C_{lift}$) with respect to Reynolds number. Figure 4.12a indicates that $C_{side}$ is dependent on Reynolds number for flow around a rectangular cylinder near a plane wall boundary. In contrast, Figures 4.12b and 4.13b show that $C_{lift}$ does not exhibit a Reynolds number dependence in either configuration. Furthermore, Figure 4.13a shows clear Reynolds number independence for a rectangular cylinder in free flow.

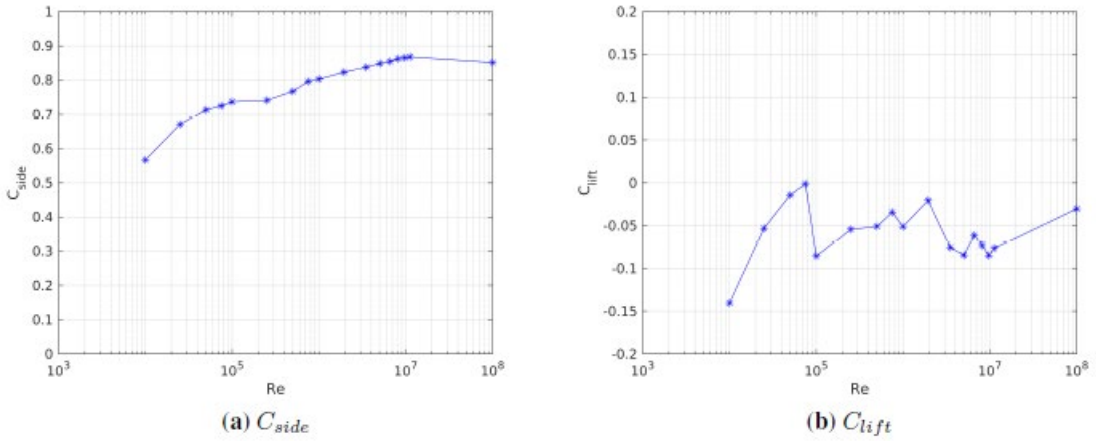


(a) $C_{side}$ (b) $C_{lift}$

**Figure 4.12 Variation of $C_{side}$ and $C_{lift}$ for flow around a rectangular cylinder near a plane wall boundary**

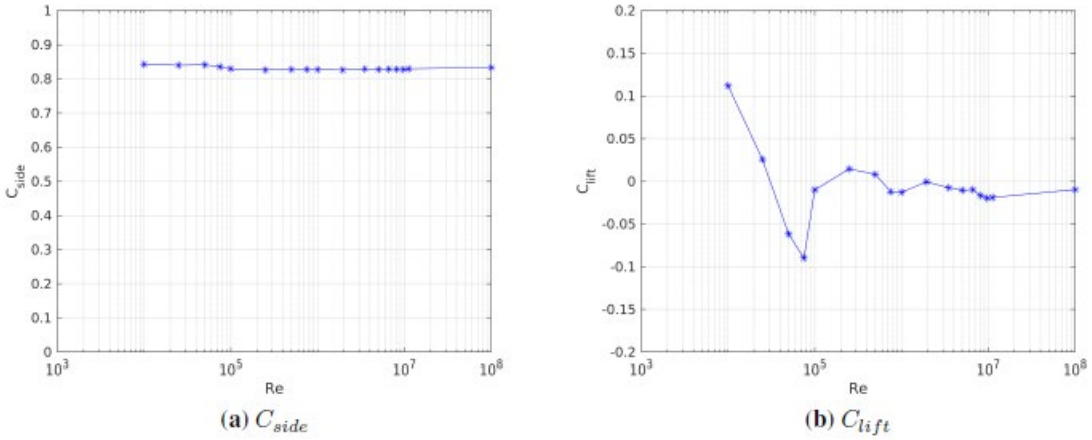


(a) $C_{side}$ (b) $C_{lift}$

**Figure 4.13 Variation of $C_{side}$ and $C_{lift}$ for flow around a rectangular cylinder in free flow**

### 4.3.3 Application to Overturning High-sided Vehicles

Figure 4.14 illustrates $C_{rolling}$ as it relates to the overturning of high-sided vehicles. Additionally, it shows that the Reynolds number dependency is relevant in $C_{rolling}$, reinforcing Equation (4.1) and revealing inaccuracies in earlier evaluations of Reynolds number dependencies concerning the overturning of high-sided vehicles (Baker 1991; Coleman and Baker 1994; Baker and Humphreys 1996).

The data shown in Figure 1.2 were analyzed for Reynolds numbers ranging from $8.5 \times 10^4$ to $1.25 \times 10^5$. Figure 4.14 demonstrates that $C_{rolling}$ depends on Reynolds number up to at least $1.12 \times 10^7$, which accounts for some of the variability observed in Figure 1.2. Furthermore, Figure 4.14 reveals that Figure 1.2 underestimates overturning values because Reynolds numbers from $8.5 \times 10^4$ to $1.25 \times 10^5$ correspond to wind speeds of 0.44 m/s (0.981 mph) to 0.64 m/s (1.442 mph).

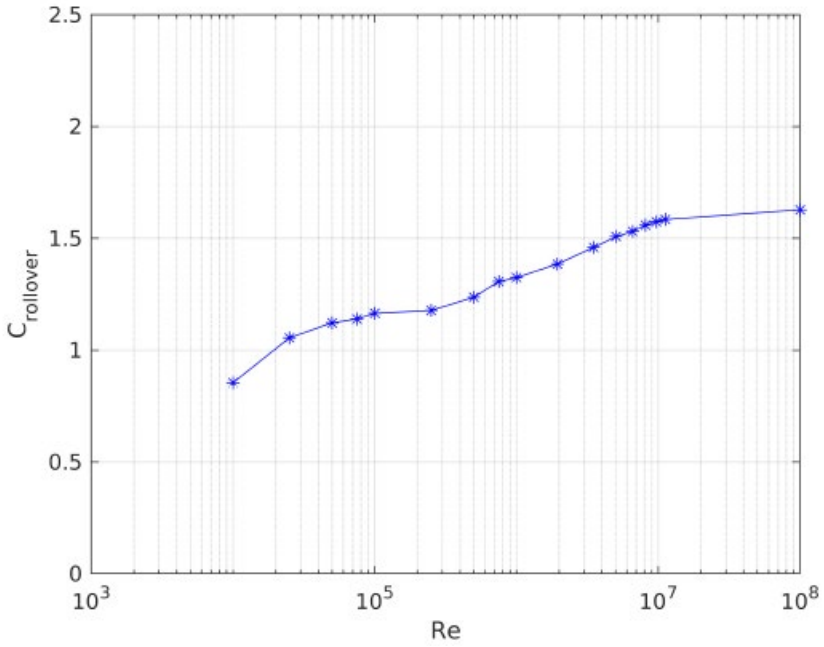


**Figure 4.14 The rolling moment coefficient $C_{rolling}$ for flow around a rectangular cylinder near a plane wall boundary as a function of Reynolds number**

Overturning crashes are more likely to occur at Reynolds numbers that are about 20 to 110 times higher than those previously considered. Realistic wind conditions correspond to full-scale wind speeds ranging from 10 m/s (22.4 mph) to 58 m/s (129.7 mph), which translate to Reynolds numbers between $1.94 \times 10^6$ and $1.12 \times 10^7$. Quantitatively, for a Reynolds number of 100,000, $C_{rolling}$ is 1.17, which is underpredicted by 19% compared with $Re = 1.94 \times 10^6$ (where $C_{rolling} = 1.39$) and by 36% compared with $Re = 1.12 \times 10^7$ (where $C_{rolling} = 1.58$). Given this Reynolds number dependency and the resulting underestimation of $C_{rolling}$ at lower Reynolds numbers, there is a clear need for further research to update analyses of overturning high-sided vehicles, ensuring that the Reynolds numbers used are realistic and that the resulting conclusions are applicable to real-world scenarios.

## 4.4 Conclusion

This study provides a comprehensive analysis that integrates two areas of research: the fundamental study of flow around rectangular cylinders near a plane wall and in free flow, and its application to the overturning of high-sided vehicles. Equation (4.1) indicates that it is premature to assume that $Re_{critical}$ has been exceeded, implying that the flow dynamics remain dependent on Reynolds numbers. In the fundamental field, $C_{drag}$ for both flow conditions has been assessed across Reynolds numbers ranging from $10^4$ to $10^8$, addressing a significant research gap. The analysis also demonstrates a strong dependence on Reynolds number for flow around a rectangular cylinder near a plane wall, particularly with a length-to-height ratio of 0.887 and a gap ratio of 0.407. In the application field, earlier studies on the overturning of high-sided vehicles need to be reassessed in light of the Reynolds number dependency demonstrated in this analysis using a 2D rectangular cylinder (Figure 4.14). It is expected that this Reynolds number dependency extends to research on 3D high-sided vehicles.

# 5. CONCLUSIONS AND FUTURE DIRECTIONS

## 5.1 Summary

This study investigated the problem of overturning high-sided vehicles through a fundamental fluid mechanics perspective. The results of this study indicate the need for a deeper analysis into the existing body of work on rolling moment coefficients ($C_{rolling}$) to further understand how it depends on Reynolds number. Chapter 2 presented a brief background on overturning high-sided vehicles, the aerodynamic coefficients of interest including $C_{rolling}$), the considerations for this study given the United States geographical focus, the background on Reynolds number dependency as it relates to an overturning high-sided vehicle, and fundamental fluid mechanics of flow around rectangular cylinders. The methods employed for this study were discussed in Chapter 3. This included the main assumptions made in the study, details on the 3D 53-GCM and 2D rectangular cylinder geometries, as well as the overall parameters that were used to set up the OpenFOAM computations.

Chapter 3 also discussed the detailed verification study that was conducted to ensure accurate CFD simulations. The drag coefficient ($C_{drag}$) was used as the basis to compare different flow domains. As a result of flow confinement around a rectangular cylinder near a plane wall boundary, three main effects that influence the domain sizing were found. An inadequate vertical domain leads to suppressed streamlines, which locally accelerate the flow and artificially increases $C_{drag}$. An adequate horizontal domain length upstream from the cylinder allows the stagnation pressure on the rectangular cylinder to propagate unimpeded to the flow inlet. Equally, a sufficient horizontal domain length downstream of the cylinder will enable the flow wake to completely develop before exiting the domain. By carefully sizing the CFD domain, a comprehensive verification study leads to high fidelity and useful results.

Chapter 4 discussed in detail the Reynolds number dependence of flow around a rectangular cylinder near a plane wall boundary and presented the application to overturning high-sided vehicles. For flow around a rectangular cylinder near a plane wall boundary with a gap ratio of 0.407, it was found that $C_{drag}$ is dependent on the flow Reynolds number. This fundamental study connects to an application field involving the overturning of high-sided vehicles, with the assumption that a 2D rectangular cylinder is representative of a high-sided vehicle's trailer section. The results from the detailed CFD studies done in this study indicate (as shown in Figure 4.14) that traditional studies on overturning high-sided vehicles assume independence of the aerodynamic coefficients such as $C_{rolling}$ on Reynolds number.

## 5.2 Conclusion

A brief discussion on the major conclusions obtained from this study follows.

Verification and validation (V&V) are fundamental requirements for performing a successful CFD study. It is common practice to assume that a grid independence study is sufficient in this regard. However, this study highlighted for high Reynolds number incompressible flow, especially for flow around a bluff body (such as a high-sided vehicle) near a plane wall boundary, the necessity to conduct a comprehensive verification analysis to ensure adequate domain sizes are chosen to enable proper flow development.

For flow around rectangular cylinders, both in free flow and near a plane wall boundary, $C_{drag}$ has been evaluated with Reynolds numbers spanning $10^4$ to $10^7$, filling a significant gap in the research. It has also been shown that there is a strong Reynolds number dependence for flow around a rectangular cylinder near a plane wall boundary, specifically with a length-to-height ratio of 0.887 and a gap ratio of 0.407.

In the application field of overturning high-sided vehicles, Equation (4.1) suggested that it is premature to assume $Re_{critical}$ has been surpassed, such that $C_{rolling}$ is Reynolds number independent. Figure 4.14 shows Reynolds number dependence for $C_{rolling}$ for flow around a rectangular cylinder near a plane wall boundary, up to at least Re = 1.12 x $10^7$. Previous work on overturning high-sided vehicles assumed Reynolds number

independence due to Re > $Re_{critical}$. Assuming the Reynolds number dependence of $C_{rolling}$, shown in Figure 4.14, carries into work investigating a 3D high-sided vehicle, previous work on overturning high-sided vehicles must be reframed.

## 5.3 Future Directions

From a fundamental perspective in the field of fluid mechanics, there is a significant research that could be conducted to inform the flow around high-sided vehicles. It would be insightful to determine the maximum gap ratio at which the flow characteristics become independent of Reynolds number such that the flow is not necessarily free flow but is also not influenced by the plane wall boundary. Conversely, it would be beneficial to reverse the analysis and investigate how a gap ratio approaching zero affects the flow dynamics and Reynolds dependency. This would be beneficial as it would support a discussion of the results discussed in Baker and Gawthorpe (1983) on Reynolds number independence. Additionally, corroborating the results of this study with experimental studies would be interesting and useful.

In the application field, it is apparent that additional work to determine $C_{rolling}$ is needed because there is a Reynolds number dependency evident in the simplified 2D analysis of flow around a rectangular cylinder near a plane wall boundary. This work needs to include the necessary extension to 3D high-sided vehicles to assess the Reynolds number dependency. The current work only explored 2D effects and naturally excluded 3D effects. Furthermore, as follow-up on this work, it would be logical to explore the effects of vehicle grouping. Extension of the present process-oriented CFD study to more representative field scale simulations would allow for a realistic understanding of the local wind field variability and the corresponding aerodynamic loads on moving vehicles, including gravitational forces. A series of simulations that are more representative of extreme windstorm conditions should also be undertaken. In summary, such CFD simulation studies will bring novel insights and inform subsequent steps involved in developing a robust decision support framework for effectively managing and operating high-sided vehicles under extreme windstorms.

# 6. REFERENCES


Baker, C. A. (1986). "Simplified analysis of various types of wind-induced road vehicle crashes." *Journal of Wind Engineering and Industrial Aerodynamics*, 22(1):69–85, 1986. doi: 10.1016/0167-6105(86)90012-7.

Baker, C., and Humphreys, N. (1996). "Assessment of the adequacy of various wind tunnel techniques to obtain aerodynamic data for ground vehicles in cross winds." *Journal of Wind Engineering and Industrial Aerodynamics*, 60:49–68, 1996. doi: 10.1016/0167-6105(96)00023-2. The Wind Engineering Society's 2nd UK Conference.

Baker, C., and Soper, D. (2022) "Calculation of the overturning wind speed of large road vehicles at exposed sites." *Proceedings of the Institution of Civil Engineers - Transport,* 175(2):97–104, 2022. doi: 10.1680/jtran.18.00102.

Bearman, P. W., and Zdravkovich, M. M. (1978). "Flow around a circular cylinder near a plane boundary." *Journal of Fluid Mechanics*, 89(1):33–47, 1978. doi: 10.1017/S002211207800244X.

Bhattacharyya, S., and Maiti, D. K. (2004). "Shear flow past a square cylinder near a wall." *International Journal of Engineering Science*, 42:2119–2134, 11 2004. doi: 10.1016/J.IJENGSCI.2004.04.0 07.

Blevins, R. D. (1984). *Applied Fluid Dynamics Handbook*. Van Nostrand Reinhold Co., New York, N.Y, 984. ISBN 0442212968.

Browand, F., McCallen, R., and Ross, J. (2009). "European Truck Aerodynamics – A Comparison Between Conventional and CoE Truck Aerodynamics and a Look into Future Trends and Possibilities." *The Aerodynamics of Heavy Vehicles II: Trucks, Buses, and Trains.* Springer.

Cheli, F., Corradi, R., Sabbioni, E., and Tomasini, G. (2011). "Wind tunnel tests on heavy road vehicles: Cross wind induced loads—part 1." *Journal of Wind Engineering and Industrial Aerodynamics*, 99(10):1000–1010, 2011. doi: 10.1016/j.jweia.2011.07.009.

Cheng, M., Whyte, D. S., and Lou, J. (2007). "Numerical simulation of flow around a square cylinder in uniform-shear flow." *Journal of Fluids and Structures*, 23:207–226, 2 2007. doi: 10.1016/J.JF LUIDSTRUCTS.2006.08.011.

Choi, H., Lee, J., and Park, H. (2014). "Aerodynamics of heavy vehicles." *Annual Review of Fluid Mechanics*, 46(1):441–468, 2014. doi: 10.1146/annurev-fluid-011212-140616.

CNN (2020). "45 semitrucks topple in 1 day due to extreme winds," https://www.cnn.com/videos/us/2020/09/09/wind-topples-semitrucks-utah-newsource-orig.cnn

Coleman, S., and Baker, C. (1990). "High sided road vehicles in cross winds." *Journal of Wind Engineering and Industrial Aerodynamics*, 36:1383–1392, 1990. doi: 10.1016/0167-6105(90)90134-X.

Coleman, S., and Baker, C. (1994). "An experimental study of the aerodynamic behaviour of high sided lorries in cross winds." *Journal of Wind Engineering and Industrial Aerodynamics*, 53(3):401–429, doi: 10.1016/0167-6105(94)90093-0.

Courchesne, J., and Laneville, A. (1979). “A comparison of correction methods used in the evaluation of drag coefficient measurements for two-dimensional rectangular cylinders.” *Journal of Fluids Engineering*, 101(4):506–510. doi: 10.1115/1.3449019.

Croll, R. H., Gutierrez, W. T., Hassan, B., Suazo, J. E., and Riggins, A. J. (1995). “Experimental investigation of the ground transportation systems (GTS) project for heavy vehicle drag reduction.” US DOE Office of Scientific and Technical Information, 12 1995.

Forouzi Feshalami, B., He, S., Scarano, F., Gan, L., and Morton, C. (2022). “A review of experiments on stationary bluff body wakes.” *Physics of Fluids*, 34(1):011301. doi: 10.1063/5.0077323.

Hoerner, S. F. (1965). *Fluid Dynamic Drag: Practical Information on Aerodynamic Drag and Hydrodynamic Resistance*. Published by the author, Midland Park, N.J.

Gerhart, P. M., Gerhart, A. L., and Hockstein, J. I. (2016). *Munson, Young and Okiishi’s Fundamentals of Fluid Mechanics*. John Wiley & Sons Inc., Hoboken, NJ, 8th edition, 2016.

Grm, A., and Batista, M. (2017). “Vehicle aerodynamic stability analysis under high crosswinds.” *Strojniški vestnik – Journal of Mechanical Engineering*, 63:191–200.

Hale, R. (2015). “History of trucking and transportation.” *TruckersLogic*. Web, Nov. 2015.

Kundu, P. K., Cohen, I. M., and Dowling, D. R. (2016). *Fluid Mechanics*. Academic Press, Boston, MA, 6th edition, 2016. ISBN 978-0-12-405935-1. doi: 10.1016/B978-0-12-405935-1.01001-7.

Mahir, N. (2009). “Three-dimensional flow around a square cylinder near a wall.” *Ocean Engineering*, 36: 357–367, 4 2009. doi: 10.1016/J.OCEANENG.2009.01.002.

Menter, F. R., (1994). “Two-equation eddy-viscosity turbulence models for engineering applications.” *AIAA J*., 32 (8), 1598–1605.

Menter, F., Kuntz, M., and Langtry, R. (2003). “Ten years of industrial experience with the SST turbulence model.” *Heat and Mass Transfer*, 4, 01.

NBC News (2017). “High Winds Topple Trucks in Colorado” https://www.nbcnews.com/news/weather/video/high-winds-topple-trucks-in-colorado-851393603623

Pope, S. B. *Turbulent Flows*. Cambridge University Press, Cambridge, 2000. ISBN 0521591252. doi: 10.1017/CBO9780511840531.

Rae, W. H., Barlow, J., and Pope, A. (1999). *Low Speed Wind Tunnel Testing*. John Wiley & Sons, Inc, New York, NY, 3rd edition. ISBN 0471557749.

Robertson, E., Choudhury, V., Bhushan, S., and Walters, D. (2015). “Validation of OpenFOAM numerical methods and turbulence models for incompressible bluff body flows.” *Computers & Fluids*, 123: 122–145, 2015. doi: 10.1016/j.compfluid.2015.09.010.

Roshko, A., Steinolfson, A., and Chattoorgoon (1975). “Flow forces on a cylinder near a wall or near another cylinder.” In *Second US National Conference on Wind Engineering Research*, pages IV–15, Jun. 1975.

Salati, L., Schito, P., Rocchi, D., and Sabbioni, E. (2018). "Aerodynamic study on a heavy truck passing by a bridge pylon under crosswinds using CFD." *Journal of Bridge Engineering*, 23(9):04018065, 2018. doi: 10.1061/(ASCE)BE.1943-5592.0001277.

Sanchez, D. K. (2023). "Investigating overturning high sided vehicles through modeling high Reynolds number incompressible flow around a rectangular cylinder near a plane wall boundary," MS Thesis, Colorado State University, 2023.

Sterling, M., Quinn, A., Hargreaves, D., Cheli, F., Sabbioni, E., Tomasini, G., Delaunay, D., Baker, C., and Morvan, H. (2010). "A comparison of different methods to evaluate the wind induced forces on a high sided lorry." *Journal of Wind Engineering and Industrial Aerodynamics*, 98(1):10–20, 2010. doi: 10.1016/j.jweia.2009.08.008.

Storms, B. L., Satran, D. R., Heineck, J. T., and Walker, S. M. "A Summary of the Experimental Results for a Generic Tractor-Trailer in the Ames Research Center 7- by 10-Foot and 12-Foot Wind Tunnels." Technical report, NASA, 2006.

TCPR (2018). "Semi rollover on Minnesota 169 closes ramp to I-494" https://www.twincities.com/2018/08/20/semi-rollover-on-minnesota-169-closes-ramp-to-i-494/

Tunay, T., Drugge, L., and O'Reilly, C. J. (2020). "On coupling methods used to simulate the dynamic characteristics of heavy ground vehicles subjected to crosswind." *Journal of Wind Engineering and Industrial Aerodynamics*, 201:104194. doi: 10.1016/j.jweia.2020.104194.

UK Government (2017). "Maximum length of vehicles used in Great Britain." UK Government. Web, Oct. 2017.

USDOT (2004). "Federal size regulations for commercial motor vehicles." US Department of Transportation, Federal Highway Administration, Office of Freight Management and Operations. Web, Oct. 2004.

Versteeg, H. K., and Malalasekera, W. (2007). *An Introduction to Computational Fluid Dynamics: The Finite Volume Method*. Pearson Education Ltd., Harlow, England, 2nd edition, 2007. ISBN 9780131274983.

WPTV (2019). "High winds from 'bomb cyclone' overturn semi on Texas highway." https://www.wptv.com/news/local-news/water-cooler/video-high-winds-from-bomb-cyclone-overturn semi-on-texas-highway

Yang, F., Zhou, Z., Tang, G., and Lu, L. (2021). "Steady flow around a square cylinder near a plane boundary." *Ocean Engineering*, 222:108599, 2 2021. doi: 10.1016/J.OCEANENG.2021.108599.

Yang, F., Peng, B., Liu, M., and Jin, X. (2022). "Large eddy simulation on a square cylinder near a plane boundary." *Ocean Engineering*, 245:109953, 2 2022. doi: 10.1016/J.OCEANENG.2021.109953.

Zdravkovich, M. (1985). "Forces on a circular cylinder near a plane wall." *Applied Ocean Research*, 7(4): 197–201, 1985. doi: 10.1016/0141-1187(85)90026-4.

Zhan, J.-m., Li, Y.-t., Wai, W.-h. O., and Hu, W.-q. (2019). "Comparison between the Q criterion and Rortex in the application of an in-stream structure." *Physics of Fluids*, 31. doi: 10.1063/1.5124245.

Zhang, Q., Su, C., Zhou, Y., Zhang, C., Ding, J., and Wang, Y. (2020). “Numerical investigation on handling stability of a heavy tractor semi-trailer under crosswind.” *Applied Sciences*, 10(11). doi: 10.3390/app10113672.